Chem Soc Rev

Solid-state electrical applications of protein and peptide based nanomaterials

Journal:	*Chemical Society Reviews*
Manuscript ID	CS-REV-11-2017-000817.R4
Article Type:	Review Article
Date Submitted by the Author:	10-Apr-2018
Complete List of Authors:	Panda, Sayak; Johns Hopkins University, Chemistry Katz, Howard; Johns Hopkins University, Materials Science and Engineering Tovar, John; Johns Hopkins University, Chemistry

Solid-state electrical applications of protein and peptide based nanomaterials

Sayak Subhra Panda[ab], Howard E. Katz[abc], John D. Tovar*[abc]

* corresponding author

[a] Department of Chemistry, Krieger School of Arts and Sciences, Johns Hopkins University, 3400 N. Charles Street, Baltimore, Maryland, 21218 United States.

[b] Institute of NanoBioTechnology, Johns Hopkins University, 3400 N. Charles Street, Baltimore, Maryland, 21218 United States.

[c] Department of Materials Science and Engineering, Whiting School of Engineering, Johns Hopkins University, 3400 N. Charles Street, Baltimore, Maryland, 21218 United States.

Abstract

The field of organic electronics continues to be driven by new charge-transporting materials that are typically processed from toxic organic solvents incompatible with biological environments. Over the past few decades, powerful examples of electron and energy transport as mediated through protein-based macromolecules have fueled the emerging area of organic bioelectronics. These attractive bioinspired architectures have enabled several important applications that draw on their functional electrical properties, ranging from field-effect transistors to piezoelectrics. In addition to naturally occurring protein biomacromolecules, unnatural oligopeptide self-assemblies and peptide-π conjugates also exhibit interesting electrical applications. This review provides an overview of electrical transport and electrical polarization in specialized biomaterials as manifested in solid-state device architectures.

Table of contents

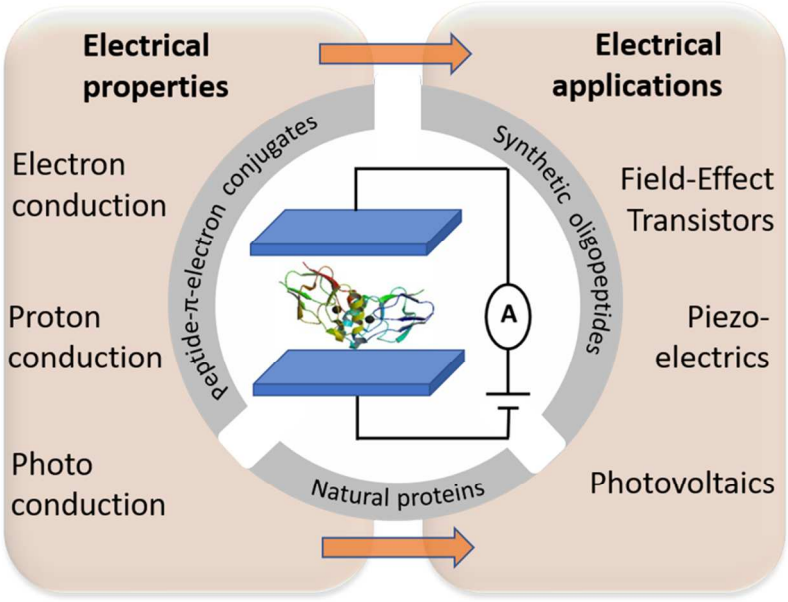

Introduction

Molecular self-assembly has enormous potential to impact research at the interface of biology, chemistry and material science as it can be used to form diverse range of nanostructures with ease.[1] Among the different biocompatible and biodegradable building blocks, self-assembling peptides and proteins are of particular interest because of their immense potential to tune functions based on nature of their assembly behavior.[2, 3] From nano-scale formation of collagen proteins to macro-scale formation of cytoskeletons, a wide range of natural structural diversity has been observed with self-assembled proteins. Peptidic biomaterials also possess other significant characteristics such as high abundance, self-healing properties, non-toxicity and antimicrobial properties. These properties have enabled self-assembled biomaterials to find use in drug delivery, bio-sensing,[4] tissue engineering[5] and artificial muscles[6]. More recently, biologically compatible nanomaterials have been developed for electronic components in the nascent area of bioelectronics, where useful electronic properties such as electron, hole and proton transport have been observed in biomaterials which have subsequently been employed in field-effect transistors (FETs), solar cells, supercapacitors and display devices.[7-10] Besides aiding in the organization of charge-transporting subunits for current-carrying devices, polypeptides are electrically polarizable and can maintain nonvolatile electric fields, which are useful properties for controlling charge densities or optical properties of adjacent materials or as means of electromechanical energy conversion. The diverse range of functionalities present in biomaterials allows for fine tuning of their natural properties in order to optimize their use in unnatural applications.[11] In this article, we provide an overview of this burgeoning field focusing on potential applications that rely on electrical properties or electronic polarization arising from peptide-based materials. We focus our attention primarily on "pure" protein and peptide structures as isolated from their natural sources or synthesized chemically, respectively. We also

touch upon solid-state electron conduction through isolated proteinaceous bacterial pili.[12] We do recognize the important and diverse nature of biological electrical transduction fostered by peptidic compositions in much more chemically heterogeneous environments such as cytochromic extrusions of bacterial filaments,[13, 14] ion channel proteins embedded within lipid bilayers,[15] and the complex components of the nervous system.[16] We aim here to highlight an orthogonal element of functional diversity and importance in the context of electrical frameworks rather than electronic properties as manifested in photophysical measurements such as UV-Vis absorbance and photoluminescence spectroscopy which have been the subject of numerous prior reports. We discuss several electrical applications of natural proteins and their variants which have been incorporated into solid state electrical devices followed related studies with synthetic/artificial small peptides and peptide-π electron conjugates. We conclude with addressing challenges to work with these soft biomaterials and future perspectives.

1. Natural proteins and mutated variants

One of the first reports of "band structure" in proteins was reported in the 1940s when photo-conduction of colored protein films was correlated with the possible existence of band structure similar to that established in inorganic semiconductors.[17, 18] Electron transfer (ET) in proteins is also of enormous interest because of the immense importance to regulate essential biological functions such as different metabolic pathways, cellular signal transduction, photosynthesis and respiration.[19] Pioneering studies of Gray and co-workers on fast long-range ET of metalloproteins in solution has encouraged further investigations on the potentially conductive nature of proteins.[20, 21] Although ET in proteins has been explored in solution since the 1960s, integration of proteins into solid-state electronics has not been investigated until more recently. One of the major obstacles to work with these soft biomaterials lies in retaining their tertiary or

quaternary structures (and thus their function) after integrating them into solid state device architectures. Another challenge is to make proper electrical connection between electrodes and proteins because proteins are made up primarily of insulating polypeptide units. However, several metalloproteins exhibit remarkable electrical properties like electron or proton transport due to the presence of redox active groups within them. These electrical properties coupled with excellent mechanical properties imported by robust peptide hierarchical structures make them excellent candidates for different electrical applications. Herein, we describe several fundamental aspects of transport characteristics of proteins in the context of solid-state electronics and then delve into different varieties of electrical applications such as FETs,[22] bio-memristors[23] and piezoelectrics[24].

Most of the work on protein conductivity focuses on a handful of protein families, namely azurin, ferritin, bacteriorhodopsin, halorhodopsin and cytochrome. Azurin is a blue copper protein which is known to mediate electron transport in bacteria via Cu redox pairs. The Cu centers are arranged in distorted trigonal bipyramidal structures with two histidine (His-117 and His-46) residues providing nitrogen coordinating sites, one cysteine (Cys-112) and one methionine (Met-121) residue providing sulfur coordinating sites and one glycine (Gly-45) residue coordinating through amide carbonyl oxygen.[25] It has been used extensively as a model for studying long range ET because of the asymmetric opposite location of the Cu centers from a surface-expressed disulfide bridge which functions as an anchor for gold substrates.[26] Ferritin is an iron-storage protein that consists of a hollow spherical peptide shell unit that encapsulates a ferric oxide core. Bacteriorhodopsin is a membrane protein which acts as a light-driven proton pump in several organisms. Although it is not known to be involved in ET in biological pathways, solid-state electron conduction was achieved because of the presence of the retinal

chromophore (**Fig. 1a**).[27] Halorhodopsins are another class of proteins where the presence of a carotenoid (bacterioruberin) and a retinal chromophore makes them similarly suitable candidates for electron conduction.[28] Cytochromes are proteins composed of different subunits with a porphyrinoid heme co-factor connected to an iron molecule within (**Fig. 1b**).[29]

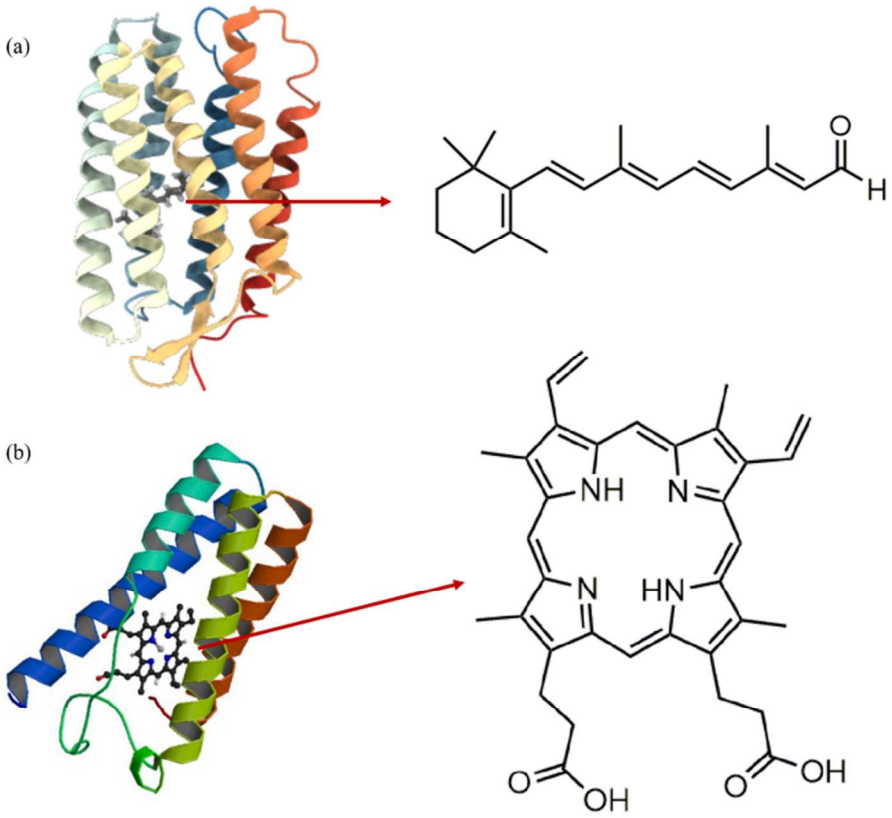

Fig. 1 Chemical structures of retinal chromophores present in bacteriorhodopsin (PDB ID: 1R2N) (a) and of porphyrinoid chromophores present in cytochrome C (PDB ID: 1RCP) (b).

(a) Electron conduction: The prospects for fast and long-range ET in proteins initiated using electrochemical and photochemical methods has prompted interest to study their electron conduction in solid-state devices. Most of the solid-state protein conduction studies rely mainly on two different approaches: (i) forming electrical contacts through single (or small ensembles of

molecules) using scanning tunneling microscopy[35] or conductive-probe atomic force microscopy[31] or (ii) through a molecular array-based approach by forming protein monolayers.[30]

To demonstrate electron transfer through small ensembles, the proteins of interest are generally adsorbed on a substrate or on the tip of a conductive probe, forming an electrical junction in between the electrodes. Zhao *et al*. studied electrical conduction and mechanical perturbation of azurin using conductive probe-atomic force microscopy (CP-AFM), where the protein was adsorbed on an Au-coated AFM tip and highly oriented pyrolytic graphite (HOPG) was used as the substrate (**Fig. 2a**).[31] The compressional force-field of the AFM tip led to variation of the current flow where electron conducting nature was attributed to the effect of quantum tunneling of electrons **(Fig. 2b).** The I-V response as a function of force modulation was rationalized through several factors such as barrier width and barrier length influencing protein structural modification. However, in this particular measurement, the junction was formed by a few molecules, not by individual proteins.

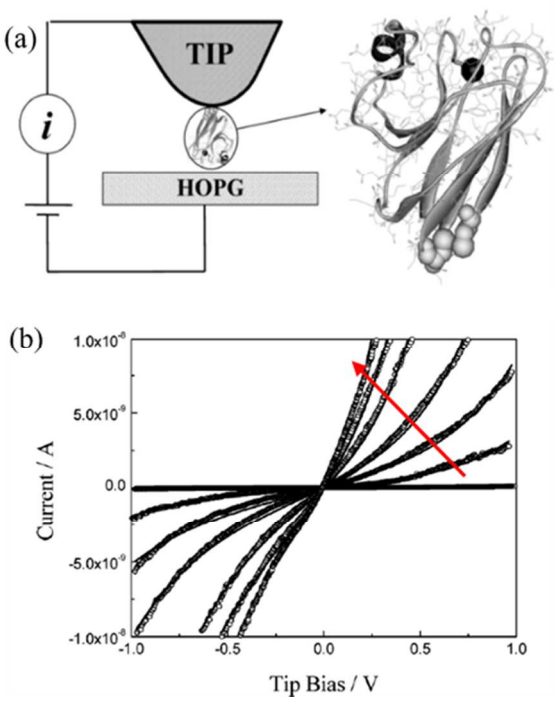

Fig. 2 (a) Schematic representation of a tip-oriented protein-HOPG junction (b) Typical I-V curve under different forces ranging from 10-55 nN (the arrow indicates an increase in force field). open circle (experimental data), solid line (theoretical modeling from modified Simmons model which is used to explain electron tunneling through organic dyes by treating the organic medium as a continuum barrier). Adapted with permission from Ref. 31. Copyright 2004 American Chemical Society.

Although the CP-AFM techniques described above provided insight about charge transport through biomacromolecules in solid-state configurations, it is of fundamental interest to examine single molecule charge transport. Xu *et al*. used similar types of methodologies with CP-AFM to demonstrate conduction through single horse spleen ferritin molecules instead of ensembles of proteins.[32] Ferritin molecules were deposited on a gold surface at a very low concentration and single protein molecules were visualized with AFM. Electrical contacts were achieved using 20 nm gold-coated AFM tips only with single protein molecules (**Fig. 3a**). Holoferritin, which

consists of a ferric oxide-phosphate mineral core and a protein shell, was found to be 5-13 times more conductive than apoferritin, where the iron core is absent, as measured using single molecular junction contact. It established that, for the ferritin protein, the core is more conductive while shell acts as a tunneling barrier for electron conduction. Similarly, single molecular charge transport of other conventional ET proteins like cytochrome P450 have been studied using CP-AFM techniques.[33] In order to monitor electron conduction through single molecules of P450, gold nano-pillars were fabricated using electron-beam lithography on the same dimensions as the diameter of protein molecules (lateral size 20-40 nm), thus ensuring attachment of single protein molecules to individual nano-pillars. The N-termini of proteins were covalently attached with an ω-thiocarboxylic acid which directed monolayer formation on the conducting gold nano-pillars through formation of Au-S linkages (**Fig. 3b**), and electrical conduction was measured upon making contact with the probe.

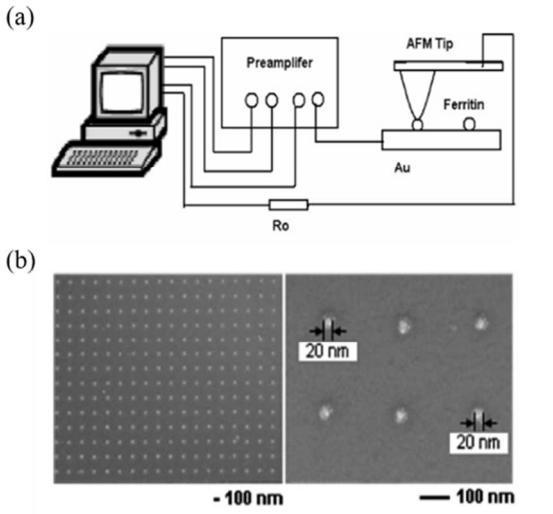

Fig. 3 (a) Set-up for I-V measurements on single ferritin molecules. Adapted with permission from Ref. 32. Copyright 2005 American Chemical Society. (b) SEM images of nanopillar arrays. Adapted with permission from Ref. 33. Copyright 2013 American Chemical Society.

The rapid development of scanning tunneling microscopy (STM) has made the study of molecular charge transport even more accessible. In this context, electrochemical STM (ECSTM) has been used to study protein ET. Schmickler *et al*. used STM to visualize redox-tunneling through iron-porphyrin molecules adsorbed on HOPG.[34] Eduardo *et al*. used STM imaging to directly visualize electron conduction in cytochrome b_{562} at different overpotentials (**Fig. 4**),[35] while electron conductance and on/off gating ratios of azurin have been studied by several groups using similar methods. However, electrical contacts could be made by either forming protein monolayers on solid substrates[36] or by absorbing the proteins on STM tips[37]. Artes *et al*. used a molecular break junction approach[38] to study electron transfer where the ECSTM tips were approached and retracted from the surface generating a probe current in between. Electron transport was found to follow first order decay depending on the distance from the junction.

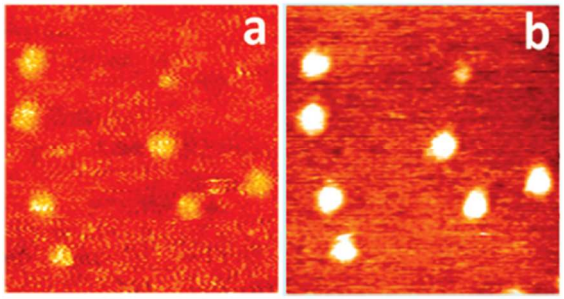

Fig. 4 ECSTM images for direct visualization of ET through seven protein molecules of cytochrome b_{562} protein at different overpotentials (a) -250 mV, (b) -10 mV. Maximum contrast is visible around -10 mV close to equilibrium redox potential of the protein. Adapted with permission from Ref. 35. Copyright 2011 American Chemical Society.

In order to fully realize the functional impact of these proteins, large-area molecular array techniques have also been explored. Ron *et al*. developed a protein monolayer junction technique

which allows large area monolayer preparation and measurement of electrical conductivity.[39] Here, the dielectric layer was modified with a suitable linker molecule that enabled covalent protein attachment. Another key feature was to use a non-destructive top electrical contact that did not alter the conformations of the proteins adsorbed to the surface. Azurin, bacteriorhodopsin and bovine serum albumin were investigated using large area monolayer formation. The azurin monolayer featured densely packed small globular particles (**Fig. 5a**), whereas the bacteriorhodopsin monolayer consisted of closely spaced fused vesicles and the bovine serum albumin monolayer exhibited relatively long particles. Azurin and bacteriorhodopsin showed significant μA currents due to their charge transporting components, whereas bovine serum albumin lacking any substantial charge transporting subunits behaved almost as an insulator with nA currents (**Fig. 5b**). The retinal chromophore present in bacteriorhodopsin was found to be a major contributor to the electron transfer through the protein whether present in a bound or unbound state. For azurin, the Cu redox center was concluded to be mainly responsible for electron conduction, because mutating it with Zn resulted in no significant current conduction. This work provided a key advancement in realizing protein-based devices based on electron transfer through monolayer protein ensembles.

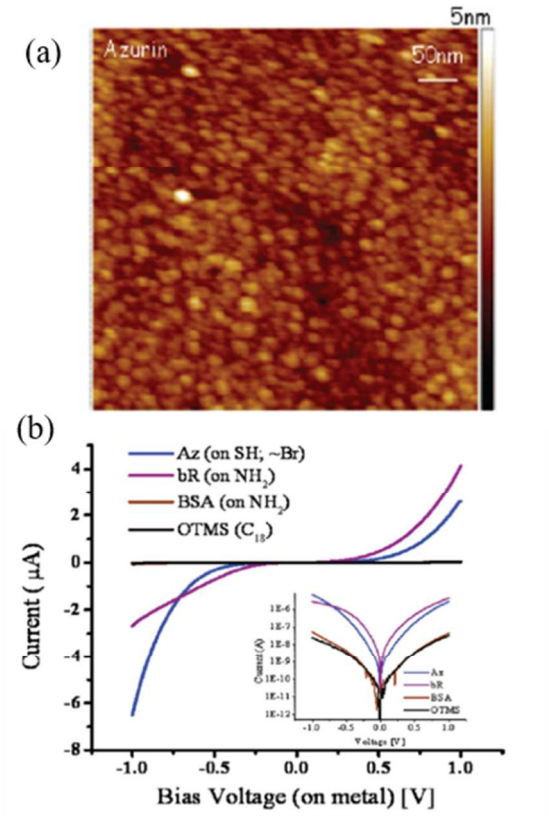

Fig. 5 (a) AFM topography image of a monolayer of azurin. (b) I-V characteristics of the three protein monolayers along with a define control octadecyltrimethoxysilane (OTMS) monolayer. Adapted with permission from Ref. 39. Copyright 2010 American Chemical Society.

Following this seminal work, the mechanisms of electron conduction through different protein monolayers were studied using the same configuration.[28, 29, 40] Temperature-variation studies of azurin ET (in the range of 80K-400K, well above the denaturation temperature of azurin) revealed that in presence of the Cu redox pair (for azurin), temperature independent behavior was obtained over a distance of 35 Å while either in absence of the Cu center (apo azurin) or after mutation with Zn (Zn-azurin), temperature-dependent transport behavior resulted (**Fig. 6a**).[40] Temperature independent ET in presence of the Cu redox pairs thus implies an activation-less tunneling through the protein which turns into thermally activated 'hopping'

mechanism without the redox-active state in the protein. Investigating the ET mechanism through cytochrome c (holo-CytC) when assembled on an H-terminated Si substrate revealed that, at room temperature, the absence of the heme group (apo-CytC) frustrates secondary structure of the protein and hence electrical transport is decreased by 3-fold from holo-CytC whereas only iron removal (porphyrin-CytC) from the protein does not alter the secondary structure and hence no significant change in transport was observed (**Fig. 6b**).[29] At higher temperature (> 195 K), a switch from tunneling type temperature independence to temperature dependence of current conduction was observed both for holo-CytC and porphyrin-CytC. Halorhodopsin was also investigated due to the presence of both retinal and carotenoid motifs which are supposed to facilitate efficient charge transport behavior.[28] A temperature-independent tunneling type ET was observed in presence of both co-factors, however, temperature dependence was recorded in the absence of any one of the cofactors which indicates a cooperative mechanism between the co-factors for electron transport (**Fig. 6c**).

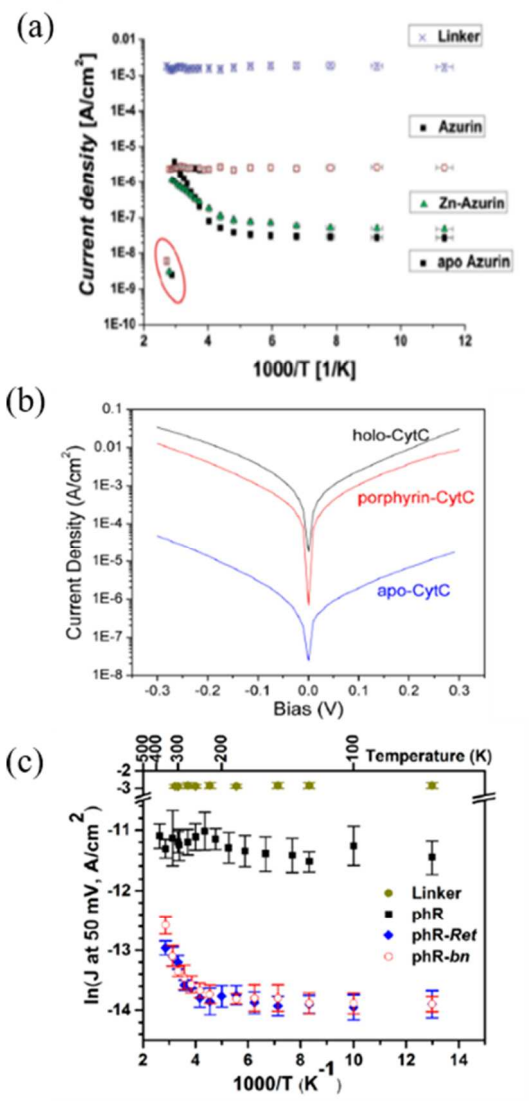

Fig. 6 (a) Current density plotted on a logarithmic scale as a function of inverse temperature for mutations of azurin. Adapted with permission from Ref. 40. Copyright 2011 American Chemical Society. (b) Room temperature current density (J) vs bias (V) curves for different CytC derivatives. Adapted with permission from Ref. 29. Copyright 2013 American Chemical Society. (c) Arrhenius plot of electron transport through monolayers of halorhodopsin (phR). phR-*Ret*: halorhodopsin without retinal chromophore, phR-*bn*: halorhodopsin without carotenoid chromophore. Adapted with permission from Ref. 28. Copyright 2015 American Chemical Society.

Rinaldi *et al*. developed an electron rectifier device from an azurin monolayer immobilized on a SiO_2 substrate. The proteins were connected to two gold nano-electrodes via sulfide bond formation with Cys3 and Cys26.[41] Both oriented and random monolayers showed rectifier behavior with a step-like current-voltage response. The presence of the Cu redox pair was critical for rectification as the device did not show any current-voltage response upon replacing it with Zn (Zn-azurin) or without any metal atom (apo-azurin).[42]

Bacterial pili also exhibit efficient electron conduction over long distances in biofilm networks and as isolated nanostructures although exact mechanism of conduction is still under debate. One scenario suggests metallic-like conductivity for pili networks of *Geobacter sulferreducens* with appropriate change in response to temperature and pH variation due to the resemblance of the characteristics of organic metals,[43] in contrast to other biologically relevant macromolecules where charge transport is generally governed by quantum-mechanical tunneling or thermally activated hopping. Vargas *et al*. genetically modified aromatic amino acid residues to alanine in pilin protein PilA resulting in loss of conductivity,[44] which was also supported by structural elucidation revealing a periodic 3.2 Å spacing in PilA proteins containing aromatic amino acid residues that was not observed upon modifying those with alanine residues.[45] Charge transport through single individual pili was also measured on gold electrodes separated by non-conductive gaps.[46] At physiologically relevant conditions (i.e. around pH 7), single pili showed conductivity around 51 $mScm^{-1}$. Modifying carboxy-terminal phenylalanine and tyrosine residues to tryptophan residues in order to incorporate efficient π-π stacking resulted in an 2000-fold increase in mean conductivity over the wild-type strain.[47] Conductivity values were also increased up to 277 Scm^{-1} under physiological conditions upon expressing the pilin monomer of *G. metallireducens* which contains more aromatic amino acids than wild-type PilA protein.[48]

Electrostatic force microscopy has also enabled the direct visualization of charge flow and distribution along individual pili of *G. sulferreducens*.[49] An alternative mechanism of electron conduction through individual pili free of metal and redox organic cofactors suggests thermally activated multistep hopping mechanism.[50,51] STM was used to probe tunneling conductance along the diameter (in contrast to the previous studies where conductivity was measured along their length) of the pili at room temperature and at a cryogenic temperature (77K) within ±1V range.[50] Band-gap feature was evident at cryogenic temperature that was absent at room temperature, which could not be attributed to only thermal broadening.

Biofilms (which are composed of pili proteins, cytochromes and other heterogeneous matter vs the isolated pili proteins described above) represent a natural medium between living cells that exhibit the unusual pili electrical properties at the macroscale. Electrical conduction through these heterogeneous biofilms also remains a subject of debate. Some studies suggest that the transport occurs via electron hopping through several outer membrane cytochrome proteins where sequences of redox reactions are responsible for the conductivity.[52] This interpretation was corroborated by theoretical calculations[53, 54] as well as *in situ* electrochemical[55, 56] and thermal[57] measurements. Recently, detailed studies on biofilms of *G. sulferreducens* as well as individual pili under similar electrochemical gating condition proposes domination of redox-current in biofilm networks whereas metallic like conductivity was confirmed for individual pili.[58] Gradual increase in conductivity of isolated pili with decrease in temperature also indicates particle-like charge carrier transport mechanism. In contrast, other studies have shown how specific modifications of the nature and concentration of pili proteins impacts biofilm conductivity rather than the extent of expression and denaturation of the cytochromes within the

biofilm and on the pili,[59, 60] suggesting that the metallic-like transport properties of the pili are ultimately responsible for the conduction.

(b) Proton Conduction: Proton conduction is an extremely important biological phenomenon which is evident from several electrochemically driven proton pumps in mitochondria, voltage-gated proton channels in phagocytes and bacterial efflux pumps. The easily tunable structural properties of proton-conducting materials are also of interest for the development of fuel cells and sensors.[61, 62] Gabriel *et al*. used a two-terminal device where a monolayer of BSA was formed at the air/water interface on Plexiglass.[62] Current flow was obtained upon making contact with platinum electrodes after applying a small voltage bias. Proton conductance depends on molecular packing: loosely bound proteins did not show significant conductance possibly due to discontinuity in contact, whereas reduction in proton conductance could be related to the changes in orientation at high packing densities. Recently, Ordinario *et al*. reported proton conductivity from reflectin, a cephalopod structural protein.[63] Two-terminal devices were constructed with both gold and hydrogenated palladium contacts where conductivity was observed at high relative humidity (90%), whereas dry reflectin channels did not show any conductivity (**Fig. 7a**). Mutating asparatate and glutamate residues in wild type reflectin to alanine also confirmed that proton conduction was dependent on carboxylic acid containing amino acids which might also play integral roles in maintaining structural integrity of the protein. Consistent gating effects were obtained from three terminal devices fabricated using PdH_x electrical contacts on a Si surface (**Fig. 7b**). Bulk protonic conductivity and mobility were measured to be around 2.6 x 10^{-3} S cm^{-1} and 7 x 10^{-3} $cm^2V^{-1}S^{-1}$, respectively, which are comparable to state-of the art proton conductors. Arrhenius-type analysis of conductivity gave an

average value of the activation energy for proton transport which was comparable to that of a hydrogen-bonded network.

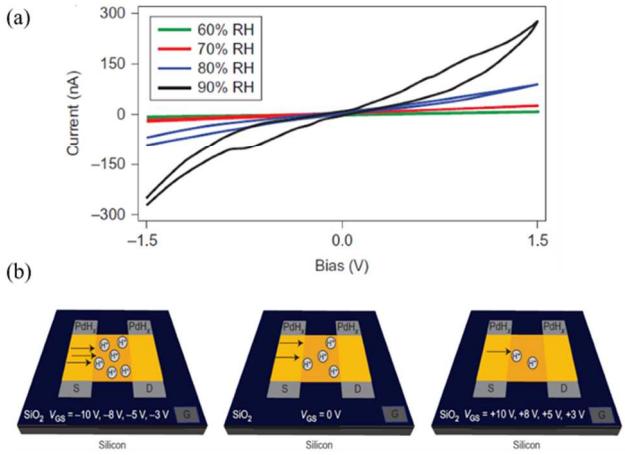

Fig. 7 (a) Electrical response of reflectin films contacted with PdH_x electrodes at different relative humidity (RH). (b) Cartoon representation of reflectin-bridged three-terminal proton-transistor at different gate-source voltage (V_{GS}). Proton current decreases from negative gate-source bias voltage to positive gate-source bias voltage. Adapted by permission from Macmillan Publishers Ltd: [Nature Chemistry] (Ref. 63), copyright 2015.

(c) Photoconduction and photovoltaics: In one of the earlier efforts to investigate photovoltaic applications with proteins, Das *et al*. demonstrated photon-harvesting from the bacterial reaction center (RC) and Photosystem I (PSI) after integrating them in solid-state devices.[64] In order to maintain protein structure and functionality, stabilizing surfactants (cationic and anionic) were used, and oriented self-assembly was achieved by modifying the proteins with histone tags (**Fig. 8a**). A protective organic semiconductor layer was also used in between the top electrode and the proteins to achieve a quantum efficiency of as high as 12% (**Fig. 8b**).

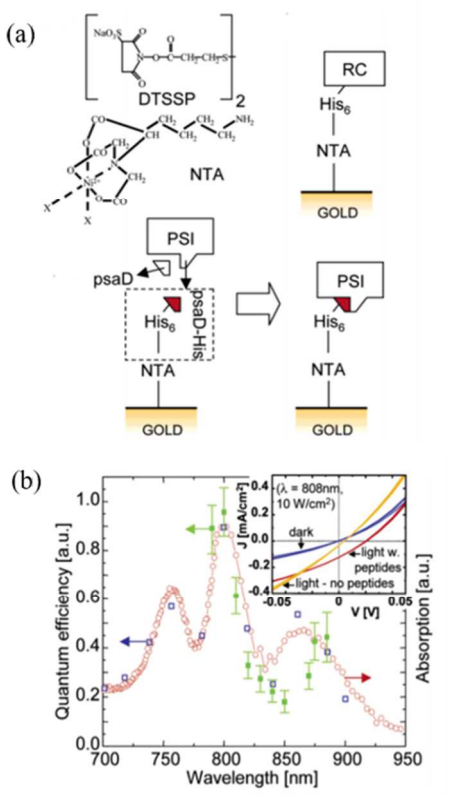

Fig. 8 (a) Techniques adapted for oriented self-assembly of proteins on gold substrates using histone tags. Gold substrates were treated with DTSSP followed by Ni^{2+}-NTA, RCs were immobilized through histone tags modified at the protein and PSIs were immobilized through exchange of native psaD with immobilized psaD-His. (b) Photocurrent spectrum of devices made from bacterial reaction center (RC). (inset) peptides employed to stabilize the protein increased photocurrent to 12% Adapted with permission from Ref. 64. Copyright 2004 American Chemical Society.

Photocurrents through single junctions of PSI were measured using near field scanning optical microscopy (NSOM) by Gerster *et al*.[65] Self-assembled monolayers on gold substrates were obtained by incorporating cysteine groups in the proteins as anchoring points and photocurrents around 10 pA were recorded. The photoconductivities of protein samples were also investigated to achieve bio-compatible opto-electronic switches. Korpany *et al*.

demonstrated photo-activity of Dronpa (a GFP protein) at the single molecule level using STM and scanning tunneling spectroscopy (STS) after assembling them onto a gold substrate.[66] Better self-assembling films were obtained by tagging histidine (6xHN) to the protein (HT-Dronpa) which ultimately resulted in better conductance. Dark-state Dronpa was found to be more conductive than the bright-state Dronpa as evident from different cycles (**Fig. 9a**), although the exact mechanism is unknown. Berthoumieu *et al*. used CP-AFM spectroscopy to investigate photoconduction of BR upon assembling it onto a gold substrate through cysteine mutation.[67] Three-fold decrease in resistance was observed under illumination with respect to the dark state (**Fig. 9b**). Mukhopadhyay *et al*. used CP-AFM to examine photoconduction of partially lipid-depleted wild-type BR proteins that formed monolayers on HOPG surfaces.[27] To investigate the mechanism and the role of specific intermediates, protein monolayers were illuminated under lights of different wavelength and current conduction was measured. Illuminating with green light resulted in a significant increase in photo-activity while adding blue light reduced it, which confirmed involvement of the "M-like" intermediate (one of the intermediates present in the BR photocycle with the greatest population at steady-state)[68], because blue light shortens the lifetime of that particular intermediate.

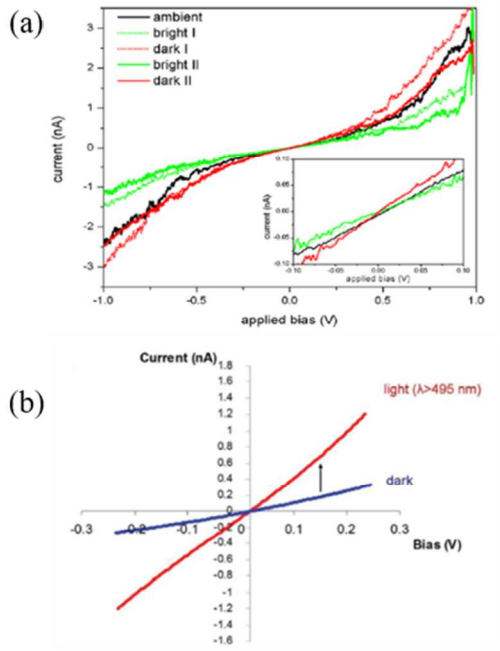

Fig. 9 (a) Averaged STS I-V spectra of HT-Dronpa as the protein is cycled through bright and dark phases. Adapted with permission from Ref. 66. Copyright 2012 American Chemical Society. (b) I-V curve of BR_{cys} in dark and under illumination using a 495nm long pass filter. Adapted with permission from Ref. 67. Copyright 2012 American Chemical Society.

(d) Field-Effect Transistors: One of the very first protein-mediated FETs was reported by Maruccio *et al*. in 2005 by taking advantage of the redox properties of blue-copper azurin protein from *P. aeruginosa* by using it as a molecular wire, which also generally shows electron transfer in biological systems (**Fig. 10a**).[22] To form a stable monolayer of the protein on a solid substrate, the SiO_2 dielectric layer was treated with 3-mercaptopropyltrimethoxysilane to obtain a layer of free thiol groups on the surface, which could then form covalent bonds with the disulfide bridges in the protein. Azurin supports two different and stable configurations of copper (i.e. Cu^{I} and Cu^{II}), and ET ability depends on the equilibrium between them. By replacing the redox active copper center with zinc, they similarly noticed no gating response as previously reported (**Fig.**

10b). A change in the behavior of the device was observed from n-type MOSFET to p-type MOSFET with respect to gate voltage which can be ascribed to the change in the relative concentration of the reduced and oxidized metallic states upon applying a gate bias. As the proteins were covalently bound to the surface, no physical displacement of the redox molecules was observed which also confirmed electron transport through a hopping mechanism as opposed to transport due to protein translocation within the monolayer. Another example of a prototype protein field effect transistor with apoferritin, the protein shell of ferritin, was reported by Yau *et al*. by simply drop-casting apoferritin in between two copper electrodes.[69]

Mentovich *et al*. investigated transport characteristics of BSA in a vertical solid-state type transistor configuration.[70] In this configuration, gold electrodes were deposited on top of the silicon dioxide layer followed by a thin layer of Si_3N_4 dielectric. Arrays of central microcavities were formed where titanium columns were evaporated, and oxide layers were grown on it to form the gate electrode. 4-nm self-assembled monolayers of BSA were deposited on top of that and palladium (Pd) layers were evaporated which served as a drain electrode in this configuration (**Fig. 10c**). Ambipolar-type transport characteristics were observed along with high gate sensitivity and low-operating voltage.

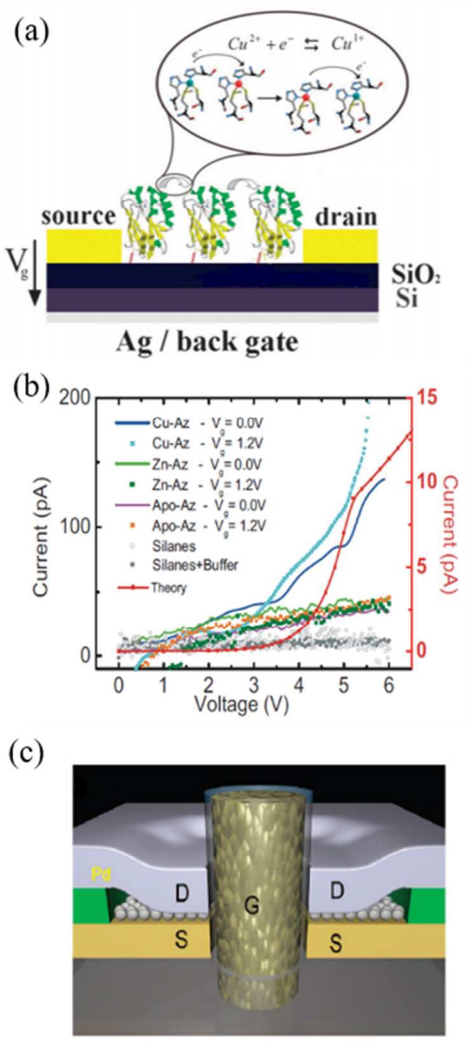

Fig. 10 (a) Transport mechanism of a protein FET. The protein monolayer is connected to Cr/Au electrodes on a SiO_2 substrate, and an Ag back-electrode is used as a gate electrode. Transport is induced by electron hopping in between the reduced and oxidized copper states. (b) Current-voltage characteristics of different variants of azurin at different voltages. Adapted from Ref. 22 with permission from John Wiley and Sons, copyright 2005. (c) Device structure of vertical solid-state protein-based transistor. S = source (gold), D = drain (palladium), G = gate (oxidized titanium column). Adapted with permission from Ref. 70. Copyright 2009 American Chemical Society.

(e) Switching memory devices: Memory devices are one of the key components of data storage systems and integrated networks, hence, the use of proteins in memory devices is next step towards realizing bio-integrated electrical systems. The new generation of memory devices are mainly focused on resistive switching between a high resistance state (HRS) to a low resistance state (LRS). Resistive switching devices based on proteins are concentrated on rewritable, nonvolatile memories although the exact mechanisms of switching vary from protein to protein.

Ferritin is an iron-storage protein which has been used extensively for resistive switching devices.[23, 71-73] Meng *et al*. designed one of the first protein-based bio-memory devices by exploiting the iron content of ferritin. Two-terminal devices were constructed by assembling ferritin molecules in between gold electrodes with a thiol linker (**Fig. 11a**) and typical I-V characteristics indicated switching from a high resistance to a low resistance value.[72] Involvement of the redox center of ferritin in the switching mechanism was confirmed by assembling apoferritin under same configuration, which lacks the active iron center and did not show any resistive switching. Oxidation and reduction of iron molecules present in the ferric-oxyhydroxyphosphate core of ferritin under the influence of the electrical bias was found to be operative for the switching mechanism (**Fig. 11b**).[73] Switching efficiency was also found to be significantly improved by assembling alternate layers of poly(allylamine hydrochloride) and ferritin.[71] A gradual increase in on/off current ratio was observed with increasing bilayer membrane, with values of the order of 10^3 obtained for devices with 15 bilayers. Kelvin force microscopy (KFM) was used to confirm the mechanism of switching which was attributed to trapping/release of charges. By applying different bias voltages at different areas of a multilayer

film, a 3D image was obtained (**Fig. 11c**). Charge trapping sites are indicted by yellow regions, whereas charge releasing states are represented by dark regions.

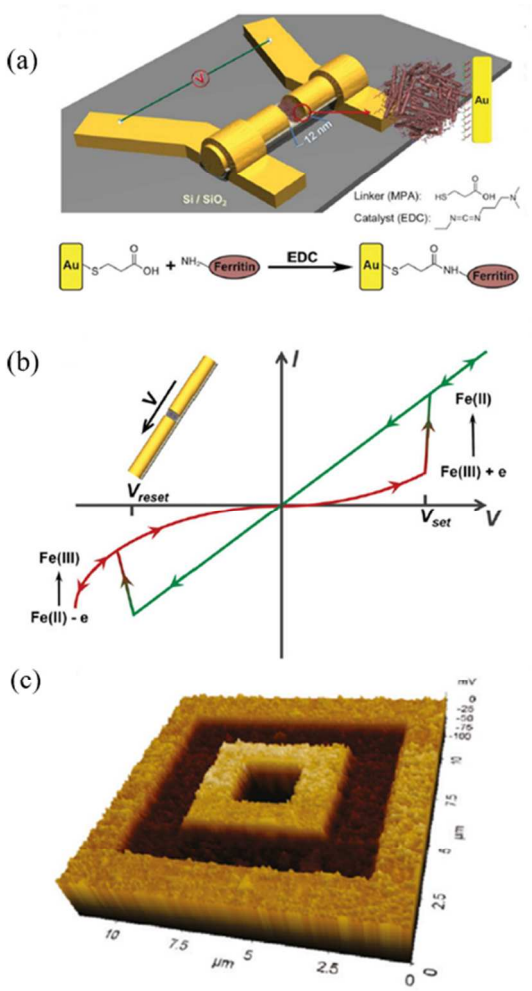

Fig. 11 (a) Schematic diagram of ferritin embedded resistive switching memory device. Adapted from Ref. 72 with permission from John Wiley and Sons, copyright 2011. (b) Schematic diagram of mechanism of ferritin based resistive switching devices. Adapted from Ref. 73 with permission from John Wiley and Sons, copyright 2014. (c) Kelvin force microscopy image of PAH/ferritin multilayers for charge trapping/release operation. Adapted with permission from Ref. 71. Copyright 2011 American Chemical Society.

Three terminal FET type memory devices have also been fabricated with ferritin nanoparticles.[74] Due to charge trapping and de-trapping of ferritin NPs in the gate dielectric layer as visualized through KFM, non-volatile memory switching was evident. A large memory window (20 V) as well as a high on/off current ratio (10^4) were obtained from these devices.

(f) Piezoelectrics: Piezoelectrics and ferroelectrics are generally made of inorganic materials and their processing generally requires higher temperatures. Most inorganic piezo- and ferroelectrics are incompatible with biological environments, which makes them unsuitable for viable bioelectric applications. Piezoelectric materials generally possess an electrical polarization upon mechanical stress, whereas ferroelectric materials require a permanent dipole along any axis of the molecule which can be reoriented by application of an external field resulting in a hysteresis loop of electrical polarization. However, both piezoelectric and ferroelectric materials require a non-centrosymmetric molecule to induce polarization.

Various biomaterials such as collagen, cellulose and silk fibers show intrinsic shear piezoelectric behavior. An early demonstration of piezoelectricity in silk fiber bundles by Fukuda *et al*. showed that electric polarization appeared in the perpendicular direction to the applied shear force.[75] Structural evidence of the piezoelectric properties of silk were further investigated by Yucel *et al*.[24] Silk undergoes structural polymorphism under mechanical stress, and the associated piezoelectric properties can be attributed to a synergistic effect of β-sheet content and molecular alignment. Silk bundles and films demonstrated piezoelectric responses of 1.0 pCN^{-1} and 1.5 pCN^{-1} respectively, an increase attributed to the enhanced molecular alignment afforded by a high-temperature zone drawing film formation technique. These values are quite comparable to those reported for quartz crystals (2 pCN^{-1}).

Lee *et al*. demonstrated the piezoelectric response of M13 bacteriophage proteins using piezoresponse force microscopy (PFM).[76] They attributed the observed piezoelectric properties to the inherent dipole moment generated by α-helical major coat proteins from the N-termini to C-termini (**Fig. 12a**). Wild-type pVIII coat proteins were mutated with different numbers of glutamate residues inducing a range of charge distributions and hence dipole moments which were correlated with increasing piezoresponses. Consistency of the experiments was validated by measuring the piezoresponse of known piezoelectric materials (i.e. periodically poled lithium niobate (PPLN) and type I collagen film) using the same set-up. A piezoelectric generator (**Fig. 12b**) was fabricated using phage films, achieving a current of the order of 6 nA (**Fig. 12c**) and a potential of 400 mV, and a liquid crystal display (LCD) was turned on using these piezoelectric generators. Shin *et al*. demonstrated axial piezoelectric response from vertically aligned M13 bacteriophage nanopillars.[77] Vertical alignment was achieved by infiltrating the phage suspension in a porous template with controllable speed. After mutating pVIII coat protein with glutamate residues, a piezoelectric response was observed from vertically aligned nanopillars that was 3-fold higher than laterally assembled bacteriophages.

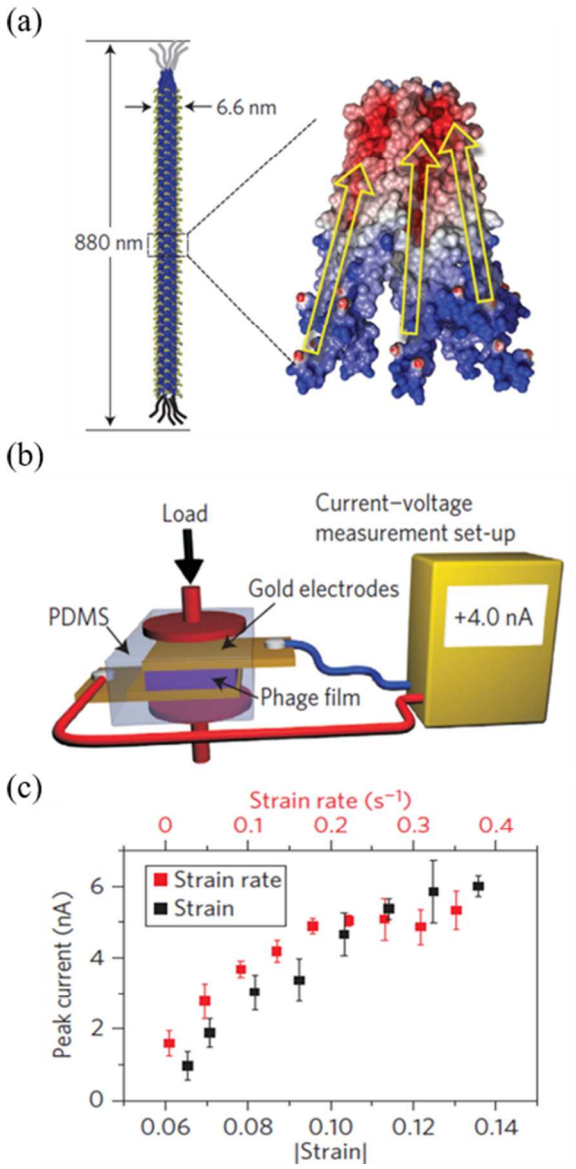

Fig. 12 (a) M13 bacteriophage has about 2700 pVIII coat proteins and five copies each of pIII and pIX proteins at either end. Electrostatic potential diagram (side view) after mutating the pVIII protein. Dipole moment is from N-terminus (blue) to C-terminus (red). (b) Schematic of piezoelectric energy generation set-up. (c) Dependence of phage based generator peak current amplitude with strain and strain rate. Strain rate is the ratio of vertical displacement of device to initial device thickness. Adapted by permission from Macmillan Publishers Ltd: [Nature Nanotechnology] (Ref. 76), copyright 2012.

Nature presents multiple examples of redox-active proteins that are made up of isolated pi-conjugated chromophores embedded within electrically "inert" protein shells. These proteins are responsible for many of the vital electron transfer processes that drive physiology and metabolism. It is therefore remarkable that monolayers and other condensed phases prepared from these electron-transfer proteins are able to exhibit electrical or proton transport in the distinctly unnatural environments of a transistor. These examples suggest a special role for the protein shell itself in modulating electrical properties, a matter addressed in the next section.

2. Synthetic oligopeptides

Small peptide oligomers also exhibit diverse properties that make them excellent candidates for nanoelectronics. Small peptides can be synthesized easily by coupling several individual amino acids in an automated fashion within a short span of time allowing for rapid screening of sequence variants. Although peptide oligomers do not have the same degree of internal structural integrity that exists within large protein macromolecules, they are suitable candidates for several applications that require electron and proton conduction, being relevant for FETs, piezoelectrics and ferroelectrics.[78]

(a) Electron and proton transport: Oligopeptides that can self-assemble into 1-D nano-tubular and fibrous structures have emerged as excellent candidates for "wire-like" charge conduction. Despite the predominantly insulating nature of the peptides, significant conduction has been observed through oligopeptides. Electron transport through small amino acids has been studied extensively using the molecular wire approach, where small molecular peptides are covalently linked to electrodes using a variety of linker molecules.[79, 80] One early example of electron conduction through oligopeptides was carried out by Slawomir and co-workers,[79] who synthesized thiol-terminated oligopeptides and established molecular junctions in between gold

electrodes and STM tips using Au-S linkages. A directional electron-transfer dependence was observed which was correlated with the electric field generated by the net molecular dipole known to be present in α-helical oligopeptides. Juhaniewicz *et al*. studied electron transmission through single amino acids (alanine, glycine and proline) connected to cystamine on both sides[80] by forming single monolayer junctions between the cystamines and the gold electrodes. These STM-based molecular junctions showed no significant difference among the three amino acids and thus ruled out any specific involvement of the side chains in electron transport.

Sepunaru *et al*. studied the role of secondary structures and amino acid composition in electron transport.[81] Homopeptides ca. 4-20 amino acids in length were synthesized from alanine, lysine, tryptophan and glutamic acid, and molecular junctions were made by incorporating a mercaptopropionic acid at the peptide N-termini (**Fig. 13a**). Peptide monolayers formed from tryptophan homopeptides showed most efficient electron transport followed by lysine, glutamic acid and alanine (**Fig. 13b**). These findings were supported by optimally tuned range-separated hybrid DFT calculations of electronic structures of homopeptides on energy minimized structures as obtained from molecular dynamics (MD) simulations. Further study revealed that conductance decreased gradually upon increasing the oligopeptide chain length of these homopeptides. Dependence on secondary structure was studied extensively by forming 20-mer alanine and lysine residues which formed helical structures. As suggested by DFT calculations, the HOMO-LUMO energy barriers for helical peptides were lower than those for the small homopeptides which was also observed experimentally.

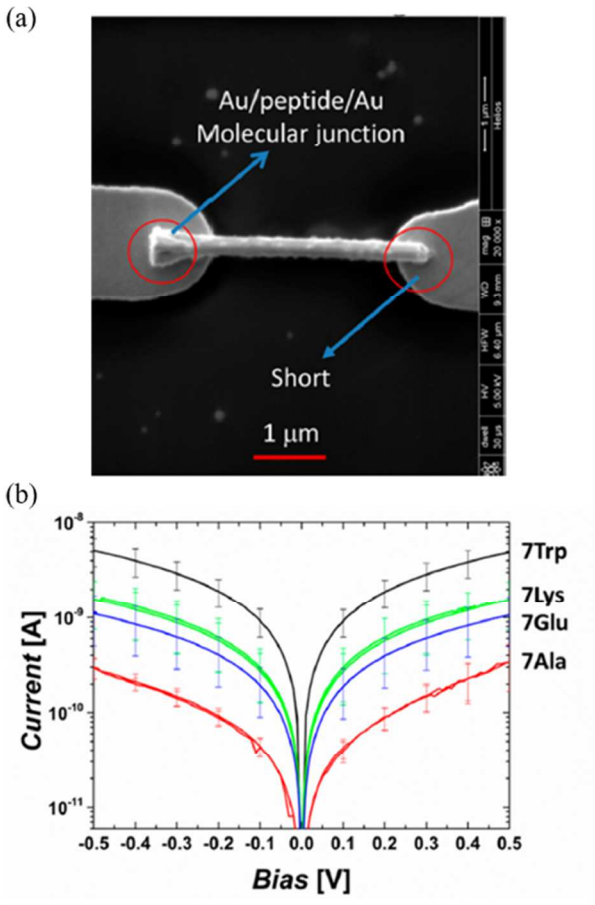

Fig. 13 (a) Scanning electron microscopy (SEM) image of Au/peptide/Au molecular junction. (b) I-V characteristics via monolayers of hepta homopeptides of Trp, Lys, Glu, Ala. Side chains of Lys & Glu are uncharged. Adapted with permission from Ref. 81. Copyright 2015 American Chemical Society.

Del Mercato *et al.* demonstrated electron conduction from an elastin related polypeptide, poly(VGGLG) which forms amyloid-like fibrils.[82] Current density was found to be dependent on the number of fibrils crossing the device junction and on the ambient environment (**Fig. 14b**). Relative humidity greatly affected the charge transport, where higher humidity (ca 70%) favors higher electrical conduction. Although the exact mechanism of transport was not established, it

was envisioned that protein hydration shells retained in the solid-state configuration facilitate charge transport in two-terminal device configurations (**Fig. 14a**).

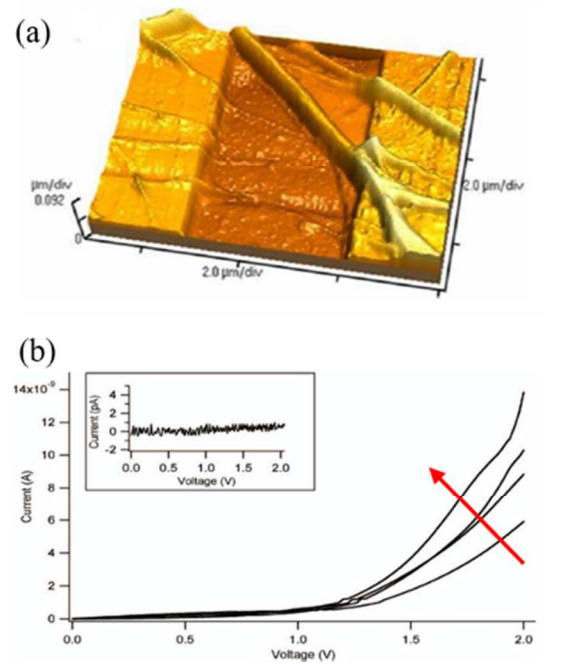

Fig. 14 (a) 3D AFM image of the poly(VGGCG) fibril across the gold electrodes. (b) I-V characteristics of the nanofibril, current depends on the number of fibrils bridging the electrodes. (inset) control experiment without the fibrils in between the electrodes (the arrow indicates an increase in number of fibrils connecting electrodes). Adapted from Ref. 82, "Copyright 2007 National Academy of Sciences".

Electrical transport behavior of diphenylalanine nanowires has also been investigated.[83] Powder x-ray diffraction suggested transformation of linear peptide molecules into cyclic configurations resulting from the formation of amide bonds in between terminal carboxylic acid and amine groups which led to efficient aromatic stacking to form herringbone-type crystalline conformations. Cyclic peptide nanotubes synthesized through vapor phase deposition showed additional red-shifted bands in diffuse reflectance spectroscopy compared to powders or linear

nanotubes prepared from aqueous diphenylalanine solutions, which was indicative of a lower optical band gap with respect to nanotubes or powders. Electrical characterization was conducted by placing the peptide nanowire in between platinum (Pt) electrodes, showing that current increased with increase in temperature indicating a semiconductor like resistivity-temperature relationship.

Mizrahi *et al.* reported charge transport through cyclic self-assembled peptide nanotubes, aligned in vertical layers in a two-terminal device where oppositely charged peptides structured in an alternating fashion.[84] Backbone hydrogen-bonding between cyclic peptides drives their self-assembly, and molecular junction formation was achieved using a CP-AFM tip as the top electrode (**Fig. 15a**). Electrical characterization of these peptides indicated probable hopping behavior for short nanotubes at lower voltage and a transfer to an electric field driven transport at higher than a threshold voltage (2.4 V) where electric field pushes the carriers along the molecules. A number of cyclic peptide nanotubes were synthesized to study proton conduction in both the dehydrated and hydrated states.[85] I-V curves were measured from nanotubes constituted of alternating lysine-tryptophan (KW), lysine-tyrosine (KY), lysine-alanine (KA), glutamic acid-tryptophan (EW) and lysine-naphthyl group capped lysine (KK_{Naph}) units (**Fig. 15b**). In dehydrated conditions, long-range ordering induced by the aromatic side chains played key roles which was evident from higher proton conduction through peptide nanotubes containing naphthyl capped lysine units. In the hydrated state, the water layer facilitates proton transport through hydrogen bonding where carboxylic acid peptide side chains exhibited highest conductivity despite having lower order of assemblies.

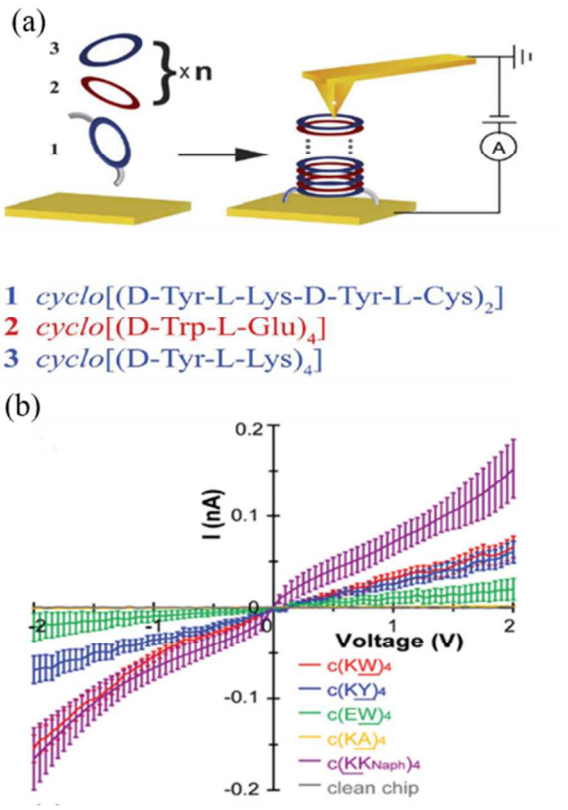

Fig. 15 (a) Schematic depiction of the assembly process of cyclic peptides. Cysteine groups attached to 1 act as an anchor to form contacts with the Au surface. Adapted from Ref. 84 with permission from Royal Society of Chemistry, copyright 2012. (b) I-V characteristics under vacuum of different cyclic peptides. Adapted from Ref. 85 with permission from Royal Society of Chemistry, copyright 2016.

Ashkenasy and co-workers mutated natural amyloid like polypeptides with unnatural amino-acids containing conjugated thienyl or furyl groups as the side chain to investigate electron transport where the two phenylalanine groups of AAKLVFF (a subunit of amyloidogenic Aβ oligopeptide) were mutated with 2-thienylalanine or 3-thienylalanine.[86, 87] Surprisingly, only for the 2-thienylalanine mutated peptide a significant increase in conductivity was observed. This was attributed to a longer range of ordering in solution when compared to the 3-thienylalanine

mutated peptide. The contributions of the aromatic side chains were established by using a non-aromatic hexa-alanine peptide which did not show any conductance despite having a similar nano-tubular structure. Furthermore, 2-furylalanine groups were incorporated in the similar peptides and compared to the 2-thienylalanine mutants.[86] Both heteroatoms in the aromatic residues did not perturb self-assembly of the peptides into fibrils, but I-V measurements in a typical two electrode configuration revealed the sheet resistance of the furan analogue was only increased by three-fold compared to the thiophene analogue. The nature of the charge transport through the 2-thienylalanine modified AAKLVFF peptides were also studied explicitly.[88] Depending on the relative humidity, the charge transport varies from a combination of proton and electron transport at lower humidity to only proton conduction at higher humidity, which was also confirmed by impedance spectroscopy measurements (**Fig. 16a**). However, aged peptide networks always showed better conduction because of the formation of better folding and self-assembly. In a similar manner, proton conduction was studied in mutated fibrils where the sequence was mutated from parent peptide (AAKLVFF) which has a basic lysine amino acid (Aβ-K), to a neutral glutamine (Aβ-Q) and acidic glutamic acid (Aβ-E) residue.[89] Peptides with acidic or basic side-chain residues showed an improvement of bulk proton conduction (**Fig. 16b**). More importantly, acidic peptides (Aβ-E) showed 28-fold increase in conductivity over the basic counterparts (Aβ-K) because of self-doping.

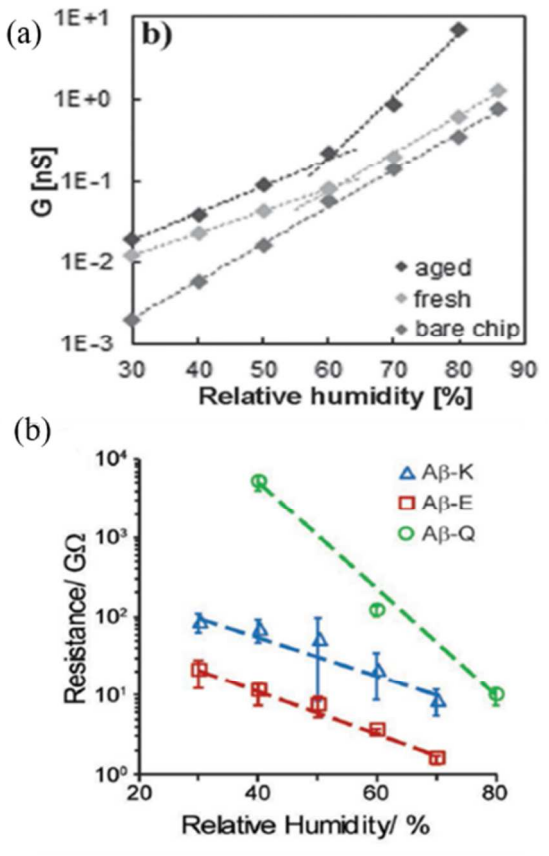

Fig. 16 (a) Conductance obtained from I-V curves as a function of relative humidity for fresh networks of peptides, aged networks, and a bare chip. Adapted from Ref. 88 with permission from John Wiley and Sons, copyright 2014. (b) Resistance vs relative humidity curve for different Aβ peptide subunits. Adapted from Ref. 89 with permission from John Wiley and Sons, copyright 2017.

(b) Piezoelectric and ferroelectric materials: Piezoelectricity refers to the capability of certain crystalline materials to convert mechanical energy into electrical energy or vice-versa. Because of the intrinsic asymmetry in bio-molecules, proteins and small peptides have been exploited to show ferroelectric behavior.[90-92]

Kholkin *et al*. demonstrated piezoelectricity from diphenylalanine peptide nanotubes which are known to form non-centrosymmetric crystals using piezo-response force microscopy (PFM) (**Fig. 17a**).[91] By performing the scan along the tube axis, an in-plane polarization component was observed which was found to be dependent on the ratio of the outer and inner radii of the nanotube (**Fig. 17b**). No out-of-plane polarization was observed suggesting the polarization component to be present only along the tube axis. As PFM only provides an idea about averaged surface vibration due to electric field distribution, a known piezoelectric material such as $LiNbO_3$ (LNO) was examined to validate this approach. Diphenylalanine nanotubes (100 nm diameter) exhibited a piezoelectric coefficient of approximately half that of bulk LNO materials (**Fig. 17c**) and considering the linear dependence between piezoresponse and diameter, a highly effective piezoelectric nature was estimated for diphenylalanine nanotubes (with diameter around 200 nm), roughly similar to classical LNO. Nguyen *et al*. reported vertical growth of highly polarized diphenylalanine nanotubes in microarrays using an external electric field,[93] which was confirmed using PFM and scanning kelvin probe microscopy. Enhanced piezoelectric response was obtained from electrically polarized nanotubes with respect to the nanotubes assembled without polarization. These nanotubes were embedded in a peptide-based power generator to obtain an open-circuit voltage of 1.4 V and a power density of 3.3 $nWcm^{-2}$, which is about 3.8 times higher than zinc-oxide nanowire-based generators. The piezoresponse of fluorenylmethyloxycarbonyl-protected diphenylalanine based hydrogels was attributed to the noncentrosymmetric β-sheet topology formed by these molecules in the gel state.[94]

Heredia *et al*. monitored polarization behavior of diphenylalanine nanotubes using PFM and second harmonic generation (SHG) techniques with varying temperature, which showed a phase-transition from non-centrosymmetric hexagonal to a possible symmetric orthorhombic structure

resulting in the disappearance of intrinsic polarity.[95] This study suggested that change in polarization behavior in diphenylalanine nanotubes could be attributed to hydrogen bonding which at higher temperature ruptures resulting in a symmetric crystal.

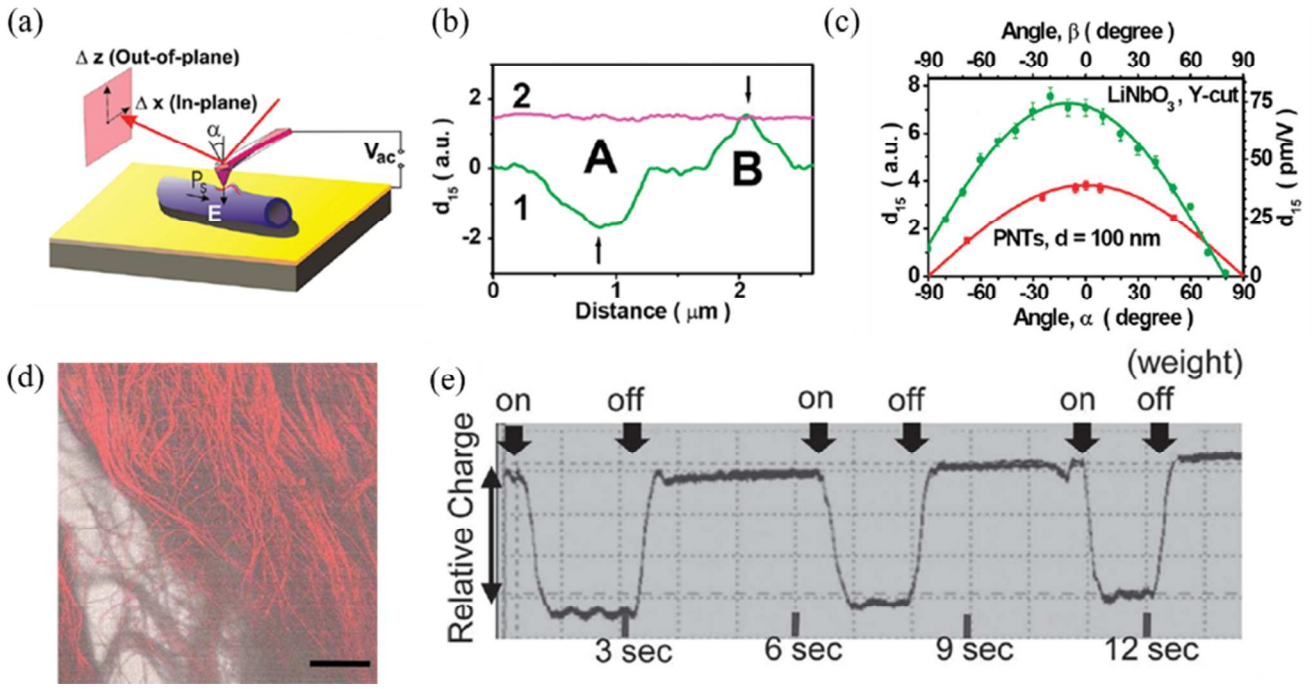

Fig. 17 (a) Schematic of the nano-scale measurements of piezoresponse force microscopy (PFM). (b) Cross-section of the in-plane PFM image along (2) and across (1) the tube axis. (c) In plane signal-angle dependence of Y-cut surface of LNO (β is the angle between the Z-axis and scanning direction) and diphenylalanine nanotubes (α is the angle between tube axis and scanning direction) of diameter 100 nm to compare shear piezoresponse of both materials (similar trend in curves allow for direct comparison of piezoelectric activities). The magnitude of piezoelectric co-efficient was calculated based on literature values of bulk LNOs. Adapted with permission from Ref. 91. Copyright 2010 American Chemical Society. (d) SHG microscopy images of electrospun poly(γ-benzyl α,L-glutamate) [PBLG] fibers. Red color is above the saturation limit of detector showing intense SHG signal. (e) Charge accumulation profile during quasistatic piezoelectric coefficient test. Adapted from Ref. 92 with permission from John Wiley and Sons, copyright 2011.

Marvin *et al*. studied the piezoelectric responses of several peptides and peptoids self-assembled on a gold substrate through mercaptopropionic acid.[96] Increasing helicity was achieved by mutating the peptide sequence from glycine to alanine to more helix-inducing aminoisobutyric acids in the backbone of the peptide. Helical structure promoting (R-(+)-α-methoxybenzyl) and structure disrupting (2-methoxyethyl) groups were varied in peptoids to induce a gradient of helicity. However, no conclusive evidence was observed correlating helicity with polarizability, but it was confirmed that peptides, due to their greater conformational flexibility, impart improved piezoelectric responses than peptoids.

Farrar *et al*. demonstrated piezoelectric properties from a composite of poly(γ-benzyl α,L-glutamate) [PBLG] and polymethylmethacrylate (PMMA) films prepared through a corona discharge method.[97] Thermal annealing led to parallel orientation of PBLG rods inside the PMMA film resulting in no piezoelectric response, whereas corona treated films oriented PBLG rods in perpendicular direction that yielded a response. They also used electrospinning to process PBLG and found a retention of the permanent helical polarity (caused by large ensemble of macroscopic dipoles due to aligned hydrogen bonding) on a macroscopic length scale.[92] Fiber X-ray diffraction and SHG microscopy confirmed parallel orientation of PBLG molecules in electrospun fibers (**Fig. 17d**). These fibers demonstrated one of the highest reported piezoelectric coefficients as observed in parallel direction for poled polymers, which was maintained even after 24 h as well as with heat treatment to 373 K (**Fig. 17e**). By combining electrospinning and a hot pressing method at about 100° C, PBLG films were prepared which showed piezoelectricity both in parallel (along long axis) as well as shear (transverse) modes.[98] The relatively lower piezoelectric coefficients along shear mode was due to the stable helical structure of PBLG films which was resistant to molecular rearrangement during the deformation process. Using

piezoelectricity in shear mode, pressure and velocity microphones have been designed by attaching PBLG fibers to Mylar films.[99]

Peptides that can undergo supramolecular association to form higher order structures are also capable of fostering electrical properties. In these cases, the pi-conjugated components of natural or unnatural origin (benzene, thiophene, indole) are much less complex than the pi-conjugated mediators used in the electron-transfer proteins (retinoids, porphyrins). Nevertheless, the extended electronic networks established within peptide nanomaterials – as mediated by pi-electron interactions or hydrogen-bonding frameworks - offer a "band structure" to promote the achievement of semiconductive properties. The following section will expand on this idea and blend the nanomaterial scaffolds enabled by small oligopeptides with the charge transport properties of extended pi-electron segments.

3. Peptide-π conjugates

The intrinsically low conductivity of biomaterials still remains one of the greatest barriers to overcome for their viability in high-performance electrical applications. Towards this end, organic π-electron rich chromophores have received significant attention as they can be easily incorporated within biologically active scaffolds to impart the necessary electronic properties.[7, 100, 101] Electrical and photonic conduction have been demonstrated through aggregates of peptide-π conjugates that have been exploited as field effect transistors (FETs) and photovoltaics (PVs).[11]

(a) Electrical conduction: Kitamura *et al*. investigated the electrical properties of tetrathiafulvalene (TTF) based organogelators using a two-probe technique in between platinum electrodes on a silicon wafer.[102] Initially, the organogelator behaved as an insulator, but after iodine doping, it showed significant conductivity. Sun *et al*. also demonstrated electrical

conduction through an anthracene based LLKK oligopeptide motif that showed a higher conductivity than pristine anthracene by itself.[103] Charge carrier mobilities of variants of peptide-conjugated naphthalene dimides (NDI) were examined by Pandeeswar *et al.*,[104] where oligopeptides forming 1D nanotapes with face-face NDI orientation in crystals showed better conductivities than the ones forming 2D nanosheets through edge-edge orientation. Khalily *et al*. also demonstrated charge transport through oligopeptides appended to pyrene and NDI groups by an alkyl chain spacer.[105] Co-mixing of two different peptides resulted in about 2400-fold and 10-fold increase in charge conductivity than the individual NDI-peptide and pyrene-peptide conjugates, respectively, which was attributed to the charge-transfer interaction between pyrene and NDI.

(b) Field-effect transistors: Many peptide-π electron conjugates used for transistor studies are based upon oligothiophene, a benchmark organic semiconductor. One of the first FETs constructed with peptide-π conjugated structures was fabricated by Wall *et al.*,[106] where quaterthiophene groups were inserted in the middle of an oligopeptide sequence and subsequent self-assembly resulted in 1-D nanostructures (**Fig. 18a**). Highly aligned hydrogels were prepared by extruding the peptides from solution which were characterized by polarized optical microscopy and scanning electron microscopy. Transistors were fabricated using these aligned peptides as active layers on silicon substrates where hole mobilities around 0.03 $cm^2V^{-1}s^{-1}$ were obtained in the parallel direction while in the perpendicular direction they were about 0.0014 $cm^2V^{-1}s^{-1}$. Stone *et al*. designed quaterthiophene and quinquethiophene peptides where the π-electron groups were linked to hydrogen-bonding peptides via alkyl chains to improve solubility. I-V characteristics and conductivities were measured using a four-point probe configuration while hole mobilities of 10^{-7} $cm^2V^{-1}s^{-1}$ were recorded from a top-contact thin-film transistor

geometry.[107] Holmes and co-workers investigated the transistor behavior of α-helical polypeptides linked to oligothiophene groups.[108] Bottom-gate, bottom contact devices were fabricated using blends of poly-peptide modified oligothiophene and phenyl-C_{60}-butyric acid methyl ester (PCBM), and hole mobilities of the order of 10^{-7} $cm^2V^{-1}s^{-1}$ were observed. Bonetti *et al*. reported a quaterthiophene based organic semiconductor covalently modified with lysine at both ends.[109] Hole mobilities around 10^{-4} $cm^2V^{-1}s^{-1}$ were obtained in a device constructed with a drop-casted active layer. Quaterthiophenes were also conjugated with different amino acids varying from glycine, alanine, valine to phenylalanine to examine the influence of amino acid substituents on the observed conductivities.[110] More hydrophobic amino-acid containing peptides showed lower conductance as measured from sheet resistance on glass substrates. Similarly, as an active layer of a transistor, maximum hole mobility was obtained from glycine-containing amino acids (**Fig. 18c**).[111] These findings were corroborated by photophysical and molecular dynamics studies that showed the smaller amino acid residues to have stronger electronic coupling.[112]

Many other π-electron motifs have also been explored as peptide-based electronic materials. Tovar and co-workers also incorporated other π-electron rich groups within peptide segments to investigate field-effect behavior (**Fig. 18b**).[113, 114] By exploiting the versatility of Pd catalyzed cross-coupling, different chain lengths of oligo-thiophenes and oligo-phenylenes were also inserted into the oligopeptide backbone.[113] Recently, more complex π-electronic units such as benzotrithiophene, decacyclene triimide and porphyrins were also embedded to extend the generality of this method to three and four-fold presentation of peptidic arms.[114]

Peptide nanostructures have also been used as gate layers on glass substrates with pentacene as an active layer to fabricate OFET devices.[111] Pentaerythritol was used as a dielectric layer in

between and, with increasing dielectric layer thicknesses, hole mobility was found to decrease as expected. Remarkably, the fields generated by the peptide gate layer were sufficient to influence the pentacene semiconductor active layer even through 50 nm of dielectric. This study demonstrated the ability of these peptide nanostructures to transmit applied biases and voltages over finite distances.

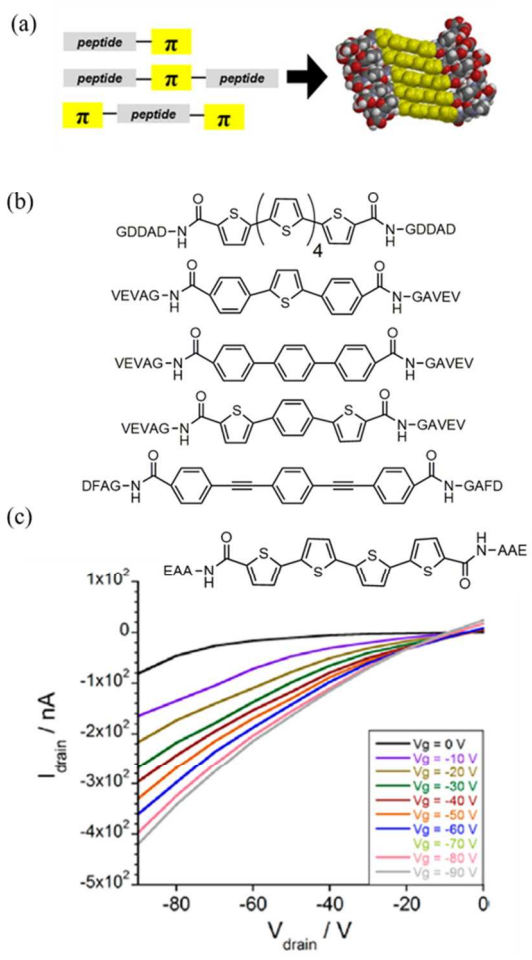

Fig. 18 (a) Schematic of peptidic 1-D nano-structures formed via self-assembly of peptide-π-electron conjugates. Adapted with permission from Ref. 11. Copyright 2015 American Chemical Society. (b) Different π-conjugated groups incorporated within peptides have been used as active layers in FETs. (c) Output curve of an OFET device prepared from the EAA-4T-AAE peptide

(depicted above the graph showing the p-channel behavior). Adapted with permission from Ref. 111. Copyright 2015 American Chemical Society.

Eakins *et al*. investigated the electrical transport properties of perylene diimide (PDI) bound to a self-assembling peptide sequence derivative from bovine Prx3 protein.[115] To investigate peptide sequence directionality effects on optoelectronic properties, two different peptides were prepared: PDI1 and PDI2 (**Fig. 19a**). Basic structures of both peptides are same which consists of a linking unit linking the PDI to the peptide backbones that consists of an adapted protein interface region and a terminal charged region to increase solubility. In PDI1 peptide, the backbone spreads from the core region with an N to C directionality whereas for the PDI2 backbone extends with a C to N orientation from the central π-region. Electronic coupling was found to be dependent on the peptide backbone directionality, as PDI1 formed efficient π-delocalized and ordered aggregates which was evident from loss of vibronic features in the UV-Vis spectra and the bisignate Cotton effect observed by CD spectroscopy. Only PDI1 showed significant transistor characteristics. Although PDI is known to behave as a n-type material, weak p-type characteristics were observed from these materials (**Fig. 19b**).

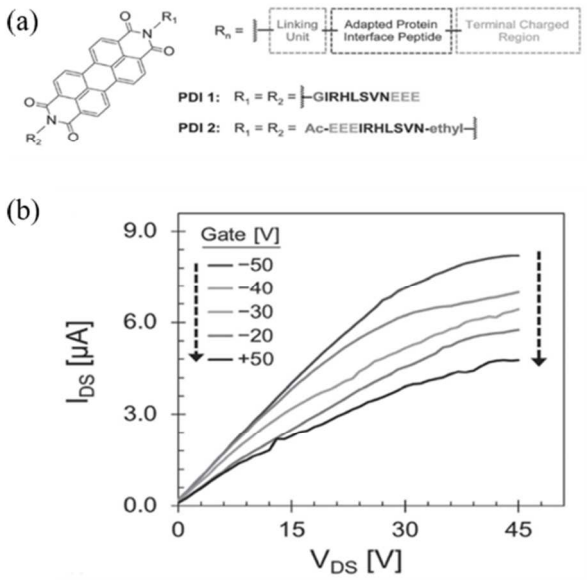

Fig. 19 (a) Different compounds investigated using peptides adapted from Prx3 protein, where PDI1 is terminated with -COOH groups and PDI2 is terminated with -NH_2 groups (b) Output characteristics of an OFET fabricated using PDI 1. Adapted from Ref. 115 with permission from John Wiley and Sons, copyright 2015.

(c) Photo-conduction: Peptide-π conjugates also exhibit photo-conductive properties upon illumination with lights of different wavelengths in UV-Vis range.[116-120] Roy *et al.* provided an initial demonstration of photo-conduction from a peptide based hydrogel, where PDI was coupled to L-tyrosine (Y) to obtain amphiphilicity.[116] Photo-response behavior was investigated after evaporating gold electrodes on PDI-Y xerogel pellets and shining light from a Xenon lamp. Significant current response was recorded for both visible light (UV-light filtered) as well as white light (UV-light unfiltered) and on/off ratios of about 18 and 51 were obtained for visible and white light respectively. Adams and co-workers have investigated into photoconduction behavior of several peptide-π conjugates. Long-lived photoconduction behavior was observed upon coupling PDI with several other amino acids.[117] An ohmic response was observed with

substantial increase upon irradiation both from PDI solutions and xerogel states formed from acidifications of these solutions. A remarkably long-lived photoconductivity was observed from a dried solution of alanine coupled PDI (ca. 5300 s) (**Fig. 20b**) that was attributed to the formation of a highly stable radical anion. Draper *et al.* also studied the photoconductive responses in diketopyrrolopyrrole (DPP) based peptide-π gelators[118] and in multicomponent xerogels composed of an electron-accepting (n-type) alanine-coupled PDI and an electron-donating stilbene-based (p-type) gelator.[120] The threshold wavelength for photoconduction in the mixed xerogel underwent a bathochromic shift to 400 nm which was attributed to the strong absorption coefficient of the stilbene group that was red-shifted upon co-mixing (**Fig. 20c**). Transient absorption spectroscopy also confirmed that the mixed xerogel was required to generate long-lived radical anions. Similarly, oligo(*p*-phenylenevinylene)s were also self-sorted with PDI based gelators by Castilla *et al.* to delve into the photoconductive responses in more complicated co-assemblies.[119]

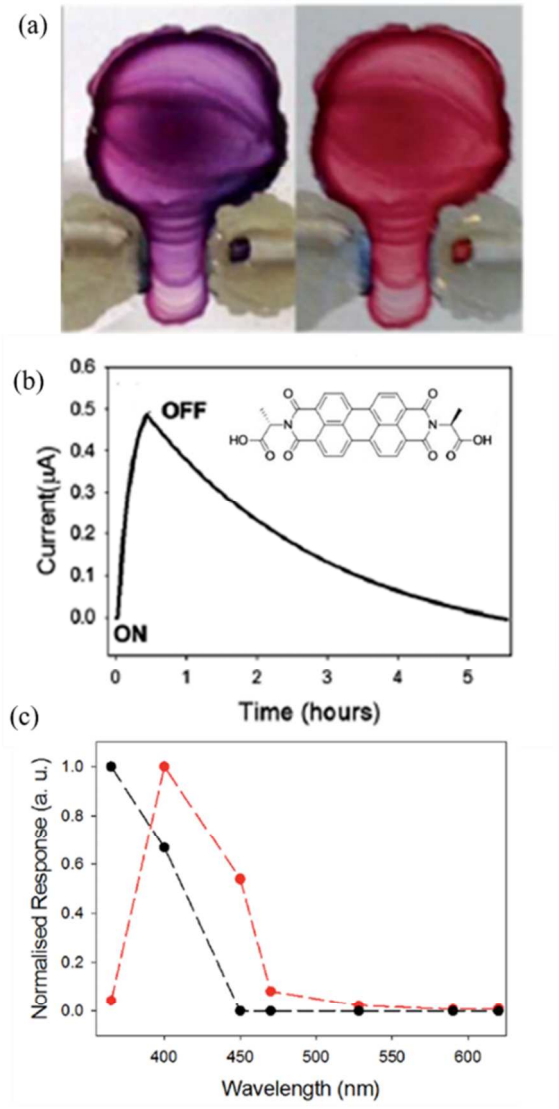

Fig. 20 (a) Xerogel of PDI-alanine upon irradiation with 365 nm light (left) changes colour, (right) original colour slowly returns after 18 hours. (b) Photoresponse of PDI-alanine gel, during irradiation with 365 nm light (from t = 0 to ca. t = 30 minutes) and subsequent decay under dark conditions. Adapted from Ref. 117 with permission from Royal Society of Chemistry, copyright 2014. (c) Normalized photocurrent of PDI-alanine only (black) and xerogel formed off PDI-alanine and OPV-phenylalanine (red). Adapted from Ref. 120 with permission from Royal Society of Chemistry, copyright 2016.

Lopez-Andarias *et al*. examined photo-current generation by co-mixing electron-donating oligo peptide-tetrathiafulvalene conjugate with electron-accepting PDI derivatives using flash-photolysis time resolved microwave conductivity measurements.[121] Photoexcitation with 355 nm laser pulse on mixed films resulted in 10 fold increase in magnitude of photoconductivity transients relative to individual films. Exciton formation and charge separation at n/p heterojunctions were rendered to be responsible for increased photo-conductivity.

(d) Photovoltaics: Holmes and co-workers fabricated bioinspired organic photovoltaic devices by blending donor quaterthiophene conjugated α-helical poly(L-lysine) described above with acceptor PCBM to form a typical D-A type heterojunction.[108] Devices were typically fabricated from 1:2 ratio of donor and acceptor to achieve an efficiency of as high as 0.22%. To compare with standard OSCs, P3HT was fabricated in the same architecture with PCBM to achieve an efficiency of only 1.24%. Although device efficiency was found to be lower than the typical OSCs, it remains a rare example of a photovoltaic device made from bio-inspired macromolecules.

Summary and Outlook

Despite their often presumed "insulating" nature, proteins and oligopeptides can be exploited for a diverse range of electrical applications. Protein and peptide-based nanomaterials with intrinsic semiconductive properties are potentially biocompatible, and they often possess thermal and mechanical stability. Various unusual applications of these materials have been explored towards the development of new tools for healthcare purposes that capitalize on their semi-conductive or other electrical functionalities. However, several key challenges still need to be addressed which include reproducible processing of these nanomaterials in solid state devices, controlling nanostructure formation on substrates, comprehending the relationship between

nanostructure morphology and electrical properties, and increasing efficiency for long term viability in ionic and biological media.

Although there are several examples of imparting electrical function to peptides or protein surfaces by way of integration with metal oxides, polymers or carbon materials, in this article we have focused on the electrical applications inherent to native proteins, peptides and peptide-pi conjugates. The advantageous features of structural diversity and sustainability make them suitable candidates towards achieving the goal of 'green' bioelectronics. Biological materials indeed provide a great platform to develop new flexible, biodegradable electronics that take advantage of the dual peptidic and electrical transporting nature of carefully engineered molecular or supramolecular systems.

Acknowledgements:

Our studies on the integration of π-conjugated systems into functional bioelectronic materials have been supported previously by the Department of Energy Basic Energy Sciences (Biomolecular Materials: DE-SC-0004857) and currently by the National Science Foundation's DMREF program (DMR-1728947).

Reference:

1. F. J. M. Hoeben, P. Jonkheijm, E. W. Meijer and A. Schenning, *Chem. Rev.*, 2005, **105**, 1491-1546.
2. L. C. Palmer and S. I. Stupp, *Acc. Chem. Res.*, 2008, **41**, 1674-1684.
3. E. Gazit, *Chem. Soc. Rev.*, 2007, **36**, 1263-1269.
4. C. A. Traina, R. C. Bakus and G. C. Bazan, *J. Am. Chem. Soc.*, 2011, **133**, 12600-12607.
5. J. Y. Wong, R. Langer and D. E. Ingber, *Proc. Natl. Acad. Sci. U.S.A*, 1994, **91**, 3201-3204.

6. J. Foroughi, G. M. Spinks, G. G. Wallace, J. Oh, M. E. Kozlov, S. L. Fang, T. Mirfakhrai, J. D. W. Madden, M. K. Shin, S. J. Kim and R. H. Baughman, *Science*, 2011, **334**, 494-497.

7. J. D. Tovar, *Acc. Chem. Res.*, 2013, **46**, 1527-1537.

8. T. Aida, E. W. Meijer and S. I. Stupp, *Science*, 2012, **335**, 813-817.

9. S. Kim, J. H. Kim, J. S. Lee and C. B. Park, *Small*, 2015, **11**, 3623-3640.

10. L. Wang, D. Chen, K. Jiang and G. Shen, *Chem. Soc. Rev.*, 2017, **46**, 6764-6815.

11. H. A. M. Ardona and J. D. Tovar, *Bioconjugate Chem.*, 2015, **26**, 2290-2302.

12. D. R. Lovley, *Curr. Opin. Electrochem.*, 2017, 190–198.

13. M. Y. El-Naggar, G. Wanger, K. M. Leung, T. D. Yuzvinsky, G. Southam, J. Yang, W. M. Lau, K. H. Nealson and Y. A. Gorby, *Proc. Natl. Acad. Sci.*, 2010, **107**, 18127–18131.

14. S. Pirbadian, S. E. Barchinger, K. M. Leung, H. S. Byun, Y. Jangir, R. A. Bouhenni, S. B. Reed, M. F. Romine, D. A. Saffarini, L. Shi, Y. A. Gorby, J. H. Golbeck and M. Y. El-Naggar, *Proc. Natl. Acad. Sci.*, 2014, **111**, 12883–12888.

15. N. Misra, J. A. Martinez, S.-C. J. Huang, Y. Wang, P. Stroeve, C. P. Grigoropoulos and A. Noy, *Proc. Natl. Acad. Sci. U. S. A.*, 2009, **106**, 13780–13784.

16. R. Chen, A. Canales and P. Anikeeva, *Nat. Rev. Mater.*, 2017, **2**, 1–16.

17. A. Szent-Györgyi, *Nature*, 1946, **157**, 875.

18. A. Szent-Gyorgyi, *Science*, 1941, **93**, 609-611.

19. R. A. Marcus and N. Sutin, *Biochim. Biophys. Acta*, 1985, **811**, 265-322.

20. J. R. Winkler and H. B. Gray, *Chem. Rev.*, 1992, **92**, 369-379.

21. H. B. Gray and J. R. Winkler, *Ann. Rev. Biochem*, 1996, **65**, 537-561.

22. G. Maruccio, A. Biasco, P. Visconti, A. Bramanti, P. P. Pompa, F. Calabi, R. Cingolani, R. Rinaldi, S. Corni, R. Di Felice, E. Molinari, M. R. Verbeet and G. W. Canters, *Adv. Mater.*, 2005, **17**, 816-822.

23. H. Wang, F. B. Meng, B. W. Zhu, W. R. Leow, Y. Q. Liu and X. D. Chen, *Adv. Mater.*, 2015, **27**, 7670-7676.

24. T. Yucel, P. Cebe and D. L. Kaplan, *Adv. Funct. Mater.*, 2011, **21**, 779-785.

25. H. Nar, A. Messerschmidt, R. Huber, M. Vandekamp and G. W. Canters, *J. Mol. Biol.*, 1991, **221**, 765-772.

26. O. Farver and I. Pecht, *J. Am. Chem. Soc.*, 1992, **114**, 5764-5767.

27. S. Mukhopadhyay, S. R. Cohen, D. Marchak, N. Friedman, I. Pecht, M. Sheves and D. Cahen, *Acs Nano*, 2014, **8**, 7714-7722.

28. S. Mukhopadhyay, S. Dutta, I. Pecht, M. Sheves and D. Cahen, *J. Am. Chem. Soc.*, 2015, **137**, 11226-11229.

29. N. Amdursky, I. Pecht, M. Sheves and D. Cahen, *J. Am. Chem. Soc.*, 2013, **135**, 6300-6306.

30. A. Vilan, D. Aswal and D. Cahen, *Chem. Rev.*, 2017, **117**, 4248-4286.

31. J. W. Zhao, J. J. Davis, M. S. P. Sansom and A. Hung, *J. Am. Chem. Soc.*, 2004, **126**, 5601-5609.

32. D. G. Xu, G. D. Watt, J. N. Harb and R. C. Davis, *Nano Lett.*, 2005, **5**, 571-577.

33. J. E. Jett, D. Lederman, L. A. Wollenberg, D. Li, D. R. Flora, C. D. Bostick, T. S. Tracy and P. M. Gannett, *J. Am. Chem. Soc.*, 2013, **135**, 3834-3840.

34. W. Schmickler and N. J. Tao, *Electrochim. Acta*, 1997, **42**, 2809-2815.

35. E. A. Della Pia, Q. J. Chi, D. D. Jones, J. E. Macdonald, J. Ulstrup and M. Elliott, *Nano Lett.*, 2011, **11**, 176-182.

36. Q. J. Chi, O. Farver and J. Ulstrup, *Proc. Natl. Acad. Sci. U.S.A*, 2005, **102**, 16203-16208.

37. A. Alessandrini, M. Salerno, S. Frabboni and P. Facci, *Appl. Phys. Lett.*, 2005, **86**.

38. J. M. Artes, I. Diez-Perez and P. Gorostiza, *Nano Lett.*, 2012, **12**, 2679-2684.

39. I. Ron, L. Sepunaru, S. Itzhakov, T. Belenkova, N. Friedman, I. Pecht, M. Sheves and D. Cahen, *J. Am. Chem. Soc.*, 2010, **132**, 4131-4140.

40. L. Sepunaru, I. Pecht, M. Sheves and D. Cahen, *J. Am. Chem. Soc.*, 2011, **133**, 2421-2423.

41. R. Rinaldi, A. Biasco, G. Maruccio, R. Cingolani, D. Alliata, L. Andolfi, P. Facci, F. De Rienzo, R. Di Felice and E. Molinari, *Adv. Mater.*, 2002, **14**, 1453-1457.

42. R. Rinaldi, A. Biasco, G. Maruccio, V. Arima, P. Visconti, R. Cingolani, P. Facci, F. De Rienzo, R. Di Felice, E. Molinari, M. P. Verbeet and G. W. Canters, *Appl. Phys. Lett.*, 2003, **82**, 472-474.

43. N. S. Malvankar, M. Vargas, K. P. Nevin, A. E. Franks, C. Leang, B. C. Kim, K. Inoue, T. Mester, S. F. Covalla, J. P. Johnson, V. M. Rotello, M. T. Tuominen and D. R. Lovley, *Nat. Nanotechnol.*, 2011, **6**, 573–579.

44. M. Vargas, N. S. Malvankar, P. L. Tremblay, C. Leang, J. A. Smith, P. Patel, O. Snoeyenbos-West, K. P. Nevin and D. R. Lovley, *mBio*, 2013, **4**, e00105–13.

45. N. S. Malvankar, M. Vargas, K. Nevin, P. L. Tremblay, K. Evans-lutterodt, D. Nykypanchuk, E. Martz, M. T. Tuominen and D. R. Lovley, *mBio,* 2015, **6**, e00084-15.

46. R. Y. Adhikari, N. S. Malvankar, M. T. Tuominen and D. R. Lovley, *RSC Adv.*, 2016, **6**, 8354–8357.

47. Y. Tan, R. Y. Adhikari, N. S. Malvankar, S. Pi, J. E. Ward, T. L. Woodard, K. P. Nevin, Q. Xia, M. T. Tuominen and D. R. Lovley, *Small*, 2016, 4481–4485.

48. Y. Tan, R. Y. Adhikari, N. S. Malvankar, J. E. Ward, T. L. Woodard, K. P. Nevin and D. R. Lovley, *mBio,* 2017, **8**, e02203-16.

49. N. S. Malvankar, S. E. Yalcin, M. T. Tuominen and D. R. Lovley, *Nat. Nanotechnol.*, 2014, **9**, 1012–1017.

50. S. Lampa-Pastirk, J. P. Veazey, K. A. Walsh, G. T. Feliciano, R. J. Steidl, S. H. Tessmer and G. Reguera, *Sci. Rep.*, 2016, **6**, 23517.

51. G. T. Feliciano, R. J. Steidl and G. Reguera, *Phys. Chem. Chem. Phys.*, 2015, **17**, 22217–22226.

52. P. S. Bonanni, D. Massazza and J. P. Busalmen, *Phys. Chem. Chem. Phys.*, 2013, **15**, 10300.

53. S. M. Strycharz-Glaven, R. M. Snider, A. Guiseppi-Elie and L. M. Tender, *Energy Environ. Sci.*, 2011, **4**, 4366.

54. H. Yan, C. Chuang, A. Zhugayevych, S. Tretiak, F. W. Dahlquist and G. C. Bazan, *Adv. Mater.*, 2015, **27**, 1908–1911.

55. M. D. Yates, S. M. Strycharz-Glaven, J. P. Golden, J. Roy, S. Tsoi, J. S. Erickson, M. Y. El-Naggar, S. C. Barton and L. M. Tender, *Nat. Nanotechnol.*, 2016, **11**, 910–913.

56. R. M. Snider, S. M. Strycharz-Glaven, S. D. Tsoi, J. S. Erickson and L. M. Tender, *Proc. Natl. Acad. Sci.*, 2012, **109**, 15467–15472.

57. M. D. Yates, J. P. Golden, J. Roy, S. M. Strycharz-Glaven, S. Tsoi, J. S. Erickson, M. Y. El-Naggar, S. Calabrese Barton and L. M. Tender, *Phys. Chem. Chem. Phys.*, 2015, **17**, 32564–32570.

58. N. Ing., T. Nusca and A. Hochbaum, *Phys. Chem. Chem. Phys.*, 2017, **19**, 21791–21799.

59. N. S. Malvankar, M. T. Tuominen and D. R. Lovley, *Energy Environ. Sci.*, 2012, **5**, 8651-8659.

60. C. Leang, N. S. Malvankar, A. E. Franks, K. P. Nevin and D. R. Lovley, *Energy Environ. Sci.*, 2013, **6**, 1901-1908.

61. E. J. Murphy, *J. Colloid Interface Sci*, 1976, **54**, 400-408.

62. B. Gabriel and J. Teissie, *Proc. Natl. Acad. Sci. U.S.A*, 1996, **93**, 14521-14525.

63. D. D. Ordinario, L. Phan, W. G. Walkup, J. M. Jocson, E. Karshalev, N. Husken and A. A. Gorodetsky, *Nat. Chem.*, 2014, **6**, 596-602.

64. R. Das, P. J. Kiley, M. Segal, J. Norville, A. A. Yu, L. Y. Wang, S. A. Trammell, L. E. Reddick, R. Kumar, F. Stellacci, N. Lebedev, J. Schnur, B. D. Bruce, S. G. Zhang and M. Baldo, *Nano Lett.*, 2004, **4**, 1079-1083.

65. D. Gerster, J. Reichert, H. Bi, J. V. Barth, S. M. Kaniber, A. W. Holleitner, I. Visoly-Fisher, S. Sergani and I. Carmeli, *Nat. Nanotechnol*, 2012, **7**, 673-676.

66. K. V. Korpany, P. Langat, D. M. Kim, N. Edelman, D. R. Cooper, J. Nadeau and A. S. Blum, *J. Am. Chem. Soc.*, 2012, **134**, 16119-16122.

67. O. Berthoumieu, A. V. Patil, W. Xi, L. Aslimovska, J. J. Davis and A. Watts, *Nano Lett.*, 2012, **12**, 899-903.

68. N. Hampp, *Chem. Rev.*, 2000, **100**, 1755-1776.

69. S. T. Yau and G. Qian, *Appl. Phys. Lett.*, 2005, **86,** 103508.

70. E. D. Mentovich, B. Belgorodsky, I. Kalifa, H. Cohen and S. Richter, *Nano Lett.*, 2009, **9**, 1296-1300.

71. Y. Ko, Y. Kim, H. Baek and J. Cho, *Acs Nano*, 2011, **5**, 9918-9926.

72. F. B. Meng, L. Jiang, K. H. Zheng, C. F. Goh, S. Lim, H. H. Hng, J. Ma, F. Boey and X. D. Chen, *Small*, 2011, **7**, 3016-3020.

73. F. B. Meng, B. Sana, Y. G. Li, Y. J. Liu, S. Lim and X. D. Chen, *Small*, 2014, **10**, 277-283.

74. B. J. Kim, Y. Ko, J. H. Cho and J. Cho, *Small*, 2013, **9**, 3784-3791.

75. E. Fukada, *J. Phys. Soc. Jpn*, 1956, **11**, 1301-1301.

76. B. Y. Lee, J. X. Zhang, C. Zueger, W. J. Chung, S. Y. Yoo, E. Wang, J. Meyer, R. Ramesh and S. W. Lee, *Nat. Nanotechnol*, 2012, **7**, 351-356.

77. D. M. Shin, H. J. Han, W. G. Kim, E. Kim, C. Kim, S. W. Hong, H. K. Kim, J. W. Oh and Y. H. Hwang, *Energy Environ Sci*, 2015, **8**, 3198-3203.

78. K. Tao, P. Makam, R. Aizen and E. Gazit, *Science*, 2017, **358**, eaam9756.

79. S. Sek, K. Swiatek and A. Misicka, *J. Phys. Chem. B*, 2005, **109**, 23121-23124.

80. J. Juhaniewicz and S. Sek, *J. Electroanal. Chem.*, 2010, **649**, 83-88.

81. L. Sepunaru, S. Refaely-Abramson, R. Lovrincic, Y. Gavrilov, P. Agrawal, Y. Levy, L. Kronik, I. Pecht, M. Sheves and D. Cahen, *J. Am. Chem. Soc.*, 2015, **137**, 9617-9626.

82. L. L. Del Mercato, P. P. Pompa, G. Maruccio, A. Della Torre, S. Sabella, A. M. Tamburro, R. Cingolani and R. Rinaldi, *Proc. Natl. Acad. Sci. U.S.A*, 2007, **104**, 18019-18024.

83. J. S. Lee, I. Yoon, J. Kim, H. Ihee, B. Kim and C. B. Park, *Angew. Chem. Int. Ed.* 2011, **50**, 1164-1167.

84. M. Mizrahi, A. Zakrassov, J. Lerner-Yardeni and N. Ashkenasy, *Nanoscale*, 2012, **4**, 518-524.

85. J. L. Yardeni, M. Amit, G. Ashkenasy and N. Ashkenasy, *Nanoscale*, 2016, **8**, 2358-2366.

86. M. Amit and N. Ashkenasy, *Isr. J. Chem.*, 2014, **54**, 703-707.

87. M. Amit, G. Cheng, I. W. Hamley and N. Ashkenasy, *Soft Matter*, 2012, **8**, 8690-8696.

88. M. Amit, S. Appel, R. Cohen, G. Cheng, I. W. Hamley and N. Ashkenasy, *Adv. Funct. Mater.*, 2014, **24**, 5873-5880.

89. O. Silberbush, M. Amit, S. Roy and N. Ashkenasy, *Adv. Funct. Mater.*, 2017, **27**, 1604624 .

90. A. Handelman, P. Beker, E. Mishina, S. Semin, N. Amdursky and G. Rosenman, *Ferroelectrics*, 2012, **430**, 84-91.

91. A. Kholkin, N. Amdursky, I. Bdikin, E. Gazit and G. Rosenman, *Acs Nano*, 2010, **4**, 610-614.

92. D. Farrar, K. L. Ren, D. Cheng, S. Kim, W. Moon, W. L. Wilson, J. E. West and S. M. Yu, *Adv. Mater.*, 2011, **23**, 3954-3958.

93. V. Nguyen, R. Zhu, K. Jenkins and R. S. Yang, *Nat. Comm.*, 2016, **7**, 13566.

94. K. Ryan, J. Beirne, G. Redmond, J. I. Kilpatrick, J. Guyonnet, N. V. Buchete, A. L. Kholkin and B. J. Rodriguez, *Acs Appl. Mater. Interfaces*, 2015, **7**, 12702-12707.

95. A. Heredia, I. Bdikin, S. Kopyl, E. Mishina, S. Semin, A. Sigov, K. German, V. Bystrov, J. Gracio and A. L. Kholkin, *J. Phys. D*, 2010, **43**, 462001.

96. C. W. Marvin, H. M. Grimm, N. C. Miller, W. S. Horne and G. W. Hutchison, *J. Phys. Chem. B*, 2017, **121**, 10269-10275.

97. D. Farrar, J. E. West, I. J. Busch-Vishniac and S. M. Yu, *Scripta Materialia*, 2008, **59**, 1051-1054.

98. K. L. Ren, W. L. Wilson, J. E. West, Q. M. Zhang and S. M. Yu, *Appl. Phys. A*, 2012, **107**, 639-646.

99. K. L. Ren, J. E. West and S. M. Yu, *J. Acoust. Soc. Am.*, 2014, **135**, EL291-EL297.

100. G. S. Vadehra, B. D. Wall, S. R. Diegelmann and J. D. Tovar, *Chem. Comm.*, 2010, **46**, 3947-3949.

101. A. M. Sanders and J. D. Tovar, *Supramol. Chem.*, 2014, **26**, 259-266.

102. T. Kitamura, S. Nakaso, N. Mizoshita, Y. Tochigi, T. Shimomura, M. Moriyama, K. Ito and T. Kato, *J. Am. Chem. Soc.*, 2005, **127**, 14769-14775.

103. Y. H. Sun, L. Jiang, K. C. Schuermann, W. Adriaens, L. Zhang, F. Y. C. Boey, L. De Cola, L. Brunsveld and X. D. Chen, *Chem. Eur. J.*, 2011, **17**, 4746-4749.

104. M. Pandeeswar, H. Khare, S. Ramakumar and T. Govindaraju, *Chem. Comm.*, 2015, **51**, 8315-8318.

105. M. A. Khalily, G. Bakan, B. Kucukoz, A. E. Topal, A. Karatay, H. G. Yaglioglu, A. Dana and M. O. Guler, *Acs Nano*, 2017, **11**, 6881-6892.

106. B. D. Wall, S. R. Diegelmann, S. M. Zhang, T. J. Dawidczyk, W. L. Wilson, H. E. Katz, H. Q. Mao and J. D. Tovar, *Adv. Mater.*, 2011, **23**, 5009-5014.

107. D. A. Stone, A. S. Tayi, J. E. Goldberger, L. C. Palmer and S. I. Stupp, *Chem. Comm.*, 2011, **47**, 5702-5704.

108. R. J. Kumar, J. M. MacDonald, T. B. Singh, L. J. Waddington and A. B. Holmes, *J. Am. Chem. Soc.*, 2011, **133**, 8564-8573.

109. S. Bonetti, A. Pistone, M. Brucale, S. Karges, L. Favaretto, M. Zambianchi, T. Posati, A. Sagnella, M. Caprini, S. Toffanin, R. Zamboni, N. Camaioni, M. Muccini, M. Melucci and V. Benfenati, *Adv. Healthc. Mater.*, 2015, **4**, 1190-1202.

110. H. A. M. Ardona, K. Besar, M. Togninalli, H. E. Katz and J. D. Tovar, J. Mater. Chem. C, 2015, **3**, 6505-6514.

111. K. Besar, H. A. M. Ardona, J. D. Tovar and H. E. Katz, *Acs Nano*, 2015, **9**, 12401-12409.

112. B. D. Wall, A. E. Zacca, A. M. Sanders, W. L. Wilson, A. L. Ferguson and J. D. Tovar, *Langmuir*, 2014, **30**, 5946-5956.

113. A. M. Sanders, T. J. Dawidczyk, H. E. Katz and J. D. Tovar, *ACS Macro Lett.*, 2012, **1**, 1326–1329.

114. A. M. Sanders, T. S. Kale, H. E. Katz and J. D. Tovar, *Acs Omega*, 2017, **2**, 409-419.

115. G. L. Eakins, R. Pandey, J. P. Wojciechowski, H. Y. Zheng, J. E. A. Webb, C. Valery, P. Thordarson, N. O. V. Plank, J. A. Gerrard and J. M. Hodgkiss, *Adv. Funct. Mater.*, 2015, **25**, 5640-5649.

116. S. Roy, D. K. Maiti, S. Panigrahi, D. Basak and A. Banerjee, *Rsc Adv.*, 2012, **2**, 11053-11060.

117. E. R. Draper, J. J. Walsh, T. O. McDonald, M. A. Zwijnenburg, P. J. Cameron, A. J. Cowan and D. J. Adams, J. Mater. Chem. C, 2014, **2**, 5570-5575.

118. E. R. Draper, B. Dietrich and D. J. Adams, *Chem. Comm.*, 2017, **53**, 1864-1867.

119. A. M. Castilla, E. R. Draper, M. C. Nolan, C. Brasnett, A. Seddon, L. L. E. Mears, N. Cowieson and D. J. Adams, *Sci. Rep.*, 2017, **7**, 8380.

120. E. R. Draper, J. R. Lee, M. Wallace, F. Jackel, A. J. Cowan and D. J. Adams, *Chem. Sci.*, 2016, **7**, 6499-6505.

121. J. Lopez-Andarias, M. J. Rodriguez, C. Atienza, J. L. Lopez, T. Mikie, S. Casado, S. Seki, J. L. Carrascosa and N. Martin, *J. Am. Chem. Soc.*, 2015, **137**, 893-897.

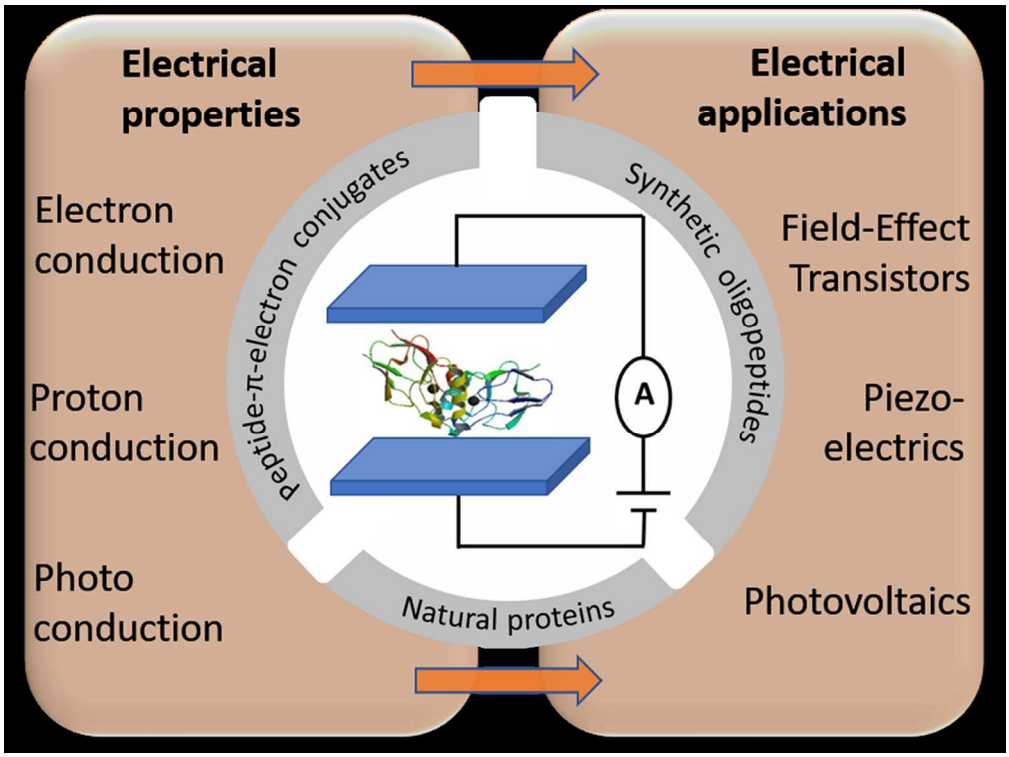

61x46mm (600 x 600 DPI)